Research Square

Preprints are preliminary reports that have not undergone peer review.
They should not be considered conclusive, used to inform clinical practice,
or referenced by the media as validated information.

Predictive Modelling of Staphylococcus aureus Growth Dynamics and Staphylococcal Enterotoxin Production in Plant-Based Çiğ köfte under Simulated Retail and Storage Temperatures in Türkiye

Mohammed Ziane
mohamed.ziane@univ-temouchent.edu.dz
Université de Ain Témouchent
Gizem Cufaoglu
Kırıkkale University
Tansu Yildiz
Kırıkkale University
Ayse Nur Erdinc
Kırıkkale University
Naim Deniz Ayaz
Kırıkkale University

Research Article

Keywords: Ready-to-eat foods, Staphylococcus aureus, Probabilistic model, Exposure assessment

Posted Date: November 25th, 2026

DOI: https://doi.org/10.21203/rs.3.rs-11761361/v1

License: This work is licensed under a Creative Commons Attribution 4.0 International License. Read Full License

Additional Declarations: No competing interests reported.

Abstract

Staphylococcus aureus is an opportunistic pathogen capable of synthesizing heat-stable enterotoxins (SEs), posing severe food safety risks in nonthermally treated ready-to-eat (RTE) matrices. Plant-based çiğ köfte is a popular Turkish RTE food characterized by high water activity (a_w>0.91) and intense manual handling during preparation and retail service. In this study, a predictive model was developed to simulate S. aureus proliferation and subsequent SE accumulation across 81 Turkish provinces under three operational scenarios: semiopen display counter service (S1), ambient room-temperature holding (S2), and secondary leftover refrigeration (S3). Primary growth kinetics derived from challenge tests with three reference strains at 22 °C (λ=0.00"-" 11.66" h" ; μ_max=0.033"-" 1.010⟦" h" ⟧^(-1)) were expanded through the Cardinal Temperature Model with Inflection (CTMI) and propagated via 10^6 Latin hypercube Monte Carlo iterations. Display counter holding (4–15 °C) maintained safe microbiological profiles during direct service, with critical threshold exceedance remaining negligible (P(C≥5.0 ⟦log_10" CFU g" ⟧^(-1))≤0.0087) and sub-toxic enterotoxin levels across both counter service (≤1.0" ng/meatball") and subsequent refrigerated leftovers (≤2.0" ng/meatball"). In contrast, unrefrigerated summer display (13–38 °C) triggered critical growth above 5.0 ⟦log_10" CFU g" ⟧^(-1), with threshold exceedance reaching 2.11% in Southeastern Anatolia, 1.66% in the Mediterranean region, 1.37% in the Aegean region, and 0.98% in Marmara. The most hazardous pathway was identified in temperature-abused ambient leftovers returned to refrigeration (S3 ex-S2), where cumulative enterotoxins reached up to 5.17⟦" ng g" ⟧^(-1) (up to 129.3" ng " per 25 g meatball), such that ingestion of a single 25 g meatball exceeded the acute intoxication threshold dose (100 ng) for sensitive populations. Sensitivity analysis identified holding temperature (r_s=+0.72" to "+0.89) and duration (r_s=+0.68" to "+0.81) as primary control targets. Risk mitigation mandates capping unrefrigerated holding at ≤2" h " during warm seasons (T≥25 ^∘ "C"), downsizing packaging units (≤5" kg"), and immediately discarding ambient leftovers.

1. INTRODUCTION

Staphylococcus aureus is among the most commonly reported bacterial pathogens involved in foodborne intoxications worldwide, largely because of its ability to produce staphylococcal enterotoxins (SEs) (Fisher et al., 2018). These toxins are responsible for food poisoning, which is characterized by sudden-onset gastrointestinal symptoms such as nausea, vomiting, and abdominal cramps (Hennekinne et al., 2012). Given its ubiquity on human skin and in the environment, *S. aureus* is considered a major concern in the production and distribution of ready-to-eat (RTE) foods, especially those that are handled manually or lack thermal treatment steps (Chieffi et al., 2023). Improper handling practices, including insufficient hand hygiene, the use of contaminated utensils, or prolonged exposure to room temperature during food preparation and retail display, can increase *S. aureus* contamination and subsequent toxin formation, particularly in foods that are consumed without further processing.

Çiğ köfte, standardized by the Turkish Standards Institution (TSE, 2018) as “Tartar A la Turca (Meatless)” under standard TS 13804, is a traditional ready-to-eat (RTE) food widely consumed across Türkiye. It consists of a bulgur base blended with spices, vegetable-derived pastes, and natural acidulants such as lemon juice and pomegranate molasses. In this study, the formulation, ingredient profile, and physicochemical quality criteria of the evaluated matrix strictly comply with these national standards. Originally, *çiğ köfte* was prepared with raw minced meat; however, following a *trichinella* outbreak linked to *çiğ köfte* consumption in İzmir, Türkiye, in 2004 (Akkoc et al., 2009), the government mandated the removal of meat from its formulation in commercial establishments. As a result, the use of raw meat in *çiğ köfte* production was banned because of public health concerns (TSE, 2018). Although it does not undergo thermal processing, it is widely distributed through both artisanal and industrial channels and is typically consumed without any further preparation. It is characterized by a pH value above 5 (Güran & İlhak, 2015; Uzunlu, 2019; Zor et al., 2025) and a water activity (a_w) exceeding 0.91 (Uzunlu, 2019), which falls within the growth range of *S. aureus* (pH: 4.0–10.0; a_w: 0.83–0.99) (ANSES, 2011). Indeed, its texture and protein-rich ingredients make it a suitable matrix for microbial survival and, under favourable conditions, bacterial growth (Gencay et al., 2016; Cagri-Mehmetoglu, 2018). In particular, the use of entirely raw ingredients and extensive manual handling during both preparation and sale increase the likelihood of introducing or sustaining opportunistic pathogens in the product.

The widespread practice of displaying *çiğ köfte* in semiopen, glass-covered retail counters, often under suboptimal refrigeration or room conditions, poses additional microbiological concerns. Moreover, although the use of gloves is mandatory, the product is typically portioned and shaped by hand during service, which further increases the risk of postprocess contamination. Depending on the region and season, the room temperature may reach levels sufficient to support the proliferation of mesophilic bacteria such as *S. aureus*. This pathogen is of particular interest in *çiğ köfte* because of its ability to survive in mildly acidic environments and in the presence of common food preservation agents, as well as its ability to produce SEs when it reaches 5 $\log_{10}$ CFU g^{-1} in foods (Zhou & Fey, 2020; Argudín et al., 2010). These toxins can accumulate without noticeable changes in sensory properties, making them a silent but significant public health threat (Cheung et al., 2021). Despite these risks, scientific data on the behavior of *S. aureus* in *çiğ köfte*, especially under varying environmental conditions, remain scarce.

Predictive microbiology and the probabilistic approach provide a structured framework for assessing such microbiological hazard levels by integrating microbial growth kinetics, environmental conditions, and consumption behaviors to estimate, in particular, human exposure to pathogens. The reliability of a quantitative exposure assessment model, however, depends on context-specific data, including initial contamination levels, growth parameters across varying temperatures, and toxin thresholds. While many similar models have been developed for other pathogens, such as *Listeria monocytogenes* (Campagnollo et al., 2018; Tirloni et al., 2018; Tsaloumi et al., 2021) and *Campylobacter* spp. (Knipper et al., 2023; Lindqvist & Lindblad, 2008), in RTE foods, there is a lack of such comprehensive modelling studies for *S. aureus* in ethnic products such as *çiğ köfte*.

To address this knowledge gap, the present study establishes a predictive approach to model *S. aureus* proliferation and subsequent staphylococcal enterotoxin (SE) accumulation in commercial, plant-based ready-to-eat (RTE) *çiğ köfte* under prevailing retail and postpurchase handling practices in Türkiye. Specifically, the model accounts for the country’s distinct bioclimatic zones, contrasting the temperate Mediterranean and Aegean coastal belts with the continental, semiarid regimes of Central and Southeastern Anatolia, where elevated ambient temperatures and seasonal heat burdens frequently challenge display-counter cooling efficiency and domestic cold-chain compliance. By coupling primary and secondary predictive growth kinetics with stochastic

time/temperature exposure profiles calibrated to these regional environments, this work determines the likelihood of staphylococcal populations reaching the critical threshold ($\geq 5.0 \log_{10}\text{:CFU:g}^{-1}$) and quantifies downstream consumer toxin exposure against critical doses.

Ultimately, this quantitative approach provides an evidence-based foundation to support targeted risk management and strengthen food safety standards governing traditional ready-to-eat (RTE) matrices across diverse geographic jurisdictions.

2. MATERIALS AND METHODS

2.1. Overview of the Study Area and Meteorological Data Sources

In this study, the model was applied at the national scale, encompassing all regions of Türkiye, to reflect the country's diverse climatic temperature conditions. Türkiye is composed of 7 geographical regions and 81 provinces. The country is geographically positioned between the subtropical and temperate zones, resulting in significant climatic variation across its regions. The Mediterranean climate, which is predominant along the southern and western coasts, is characterized by hot, dry summers and mild, rainy winters. In contrast, the Black Sea climate prevails along the northern coastline, featuring cool summers and relatively warm, wet winters in coastal areas, whereas the inland and elevated zones experience colder and snowier conditions. The Central Anatolian regions are dominated by a continental (or terrestrial) climate, marked by pronounced temperature differences between day and night as well as between seasons. Finally, the Marmara Region has a transitional climate that incorporates features of the Mediterranean, Black Sea, and continental climates, reflecting its unique geographic position at the intersection of multiple climatic zones. Table 1 summarizes the range between the median minimum ($T_{\text{med-min}}$) and median maximum ($T_{\text{med-max}}$) monthly temperatures (°C) across the seven regions of Türkiye. The daily room temperatures were collected for the year 2025 from https://www.accuweather.com/ for all 81 cities in the seven regions.

Table 1
Seasonal room temperature (T_{room}, °C) ranges across geographical regions in Türkiye parameterized for the *çiğ köfte* exposure model (2025).

Geographical Region (i)	Winter (j = 1)		Spring (j = 2)		Summer (j = 3)		Autumn (j = 4)	
	$T_{\text{med}-\text{min}}$	$T_{\text{med}-\text{max}}$	$T_{\text{med}-\text{min}}$	$T_{\text{med}-\text{max}}$	$T_{\text{med}-\text{min}}$	$T_{\text{med}-\text{max}}$	$T_{\text{med}-\text{min}}$	$T_{\text{med}-\text{max}}$
Eastern Anatolia ($i = 1$)	0	4	4	17	13	31	4	20
Central Anatolia ($i = 2$)	0	8	6	18	16	31	7	20
Black Sea ($i = 3$)	1	9	6	18	16	30	11	21
Marmara ($i = 4$)	2	12	8	20	19	33	12	21
Aegean ($i = 5$)	2	12	8	21	19	35	11	23
Southeastern Anatolia ($i = 6$)	0	11	9	23	21	38	11	25
Mediterranean ($i = 7$)	4	14	10	24	22	35	14	27

Note: Values represent regional seasonal medians of daily minimum (T_{min}) and maximum (T_{max}) temperatures compiled across 81 provinces from meteorological datasets (https://www.accuweather.com/). In Scenario 2, holding temperatures are sampled as $T_{\text{room},i,j} \sim \text{Uniform}\left(T_{\text{med}-\text{min},i,j}, T_{\text{med}-\text{max},i,j}\right)$ with geographical region ($i = 1, ..., 7$) and season ($j = 1, ..., 4$).

2.2. Model overview and bacterial selection

Data on *çiğ köfte* preparation and serving practices were collected through preliminary visits to more than 15 retail shops and through consultations with more than 15 experts. These data were used to define the scenarios from which the predictive model for this study was developed. Thus, the present predictive model was developed by integrating both realistic scenarios (e.g., observed service times and temperatures) and hypothetical scenarios (e.g., expert-based assumptions and fitted distributions of time and temperature) that influence the growth of *S. aureus* in *çiğ köfte* up to the point of consumption. The amount of enterotoxin produced per consumed meatball was subsequently predicted. The product is not subjected to heat processing. Thus, in this study, only storage and service time/temperature were considered to model bacterial growth from the initial concentration of *S. aureus* at the time of package opening to the time of consumption. The factors evaluated in the model include (i) initial contamination level, (ii) storage/serving temperature, (iii) service/waiting time, and (iv) strain-specific growth parameters (lag time and growth rate). These were assessed using literature data, expert opinions, and challenge test results. The model includes two modules: the initial concentration module (H_0) and the growth module (Gi) under different temperature/time scenarios. The output is the estimated *S. aureus* concentration ($\log_{10}$ CFU g^{-1}) at different time points with the prediction of SE production. The model is designed to simulate the individual servings of *çiğ köfte*. Consequently, the input distributions (e.g., for initial contamination and growth parameters) primarily represent the inherent variability across these servings while also encompassing some parameter uncertainty. This approach is more informative, as it allows for the estimation of highly critical situations of servings that a model based on mean values would obscure.

2.3. Exposure Assessment: Supply Chain Stages and Exposure Scenarios

This exposure assessment evaluated commercial ready-to-eat (RTE) meatless *çiğ köfte* distributed through retail shops across Türkiye (Fig. 1). In the commercial supply chain, *çiğ köfte* is manufactured in centralized production facilities, vacuum packaged into commercial containers, and dispatched to retail outlets via refrigerated transport vehicles. Although *S. aureus* is generally considered a weak competitor under strict anaerobiosis, its facultative anaerobic physiology enables survival and limited metabolic activity in vacuum-packaged RTE food systems during extended distribution (Ingham et al., 2005).

Upon retail delivery, unopened vacuum packages are maintained under commercial cold storage ($T_{\text{cold}} \sim \text{Uniform}(4\,^{\circ}\text{C},\ 8\,^{\circ}\text{C})$) for an average holding interval of $t_{\text{cold}} \leq 96\ \text{h}$(4 days) across wholesale storage and retail inventory. Because *S. aureus* growth can occur during prolonged cold storage, the model accounted for potential lag time completion during this predisplay phase.

The retail display and consumption timeline begins when vacuum packages are opened and transferred onto display trays, representing the baseline simulation time ($t_0 = 0\ \text{h}$). Retail outlets typically commence operations at 10:00 AM, at which point commercial batches ($W_{\text{package}} = 10{,}000\ \text{g}$) are spread onto showcase counters and covered with polyethylene food-grade cling film. Because *çiğ köfte* is predominantly consumed as an appetizer or main course during lunch and dinner, consumer exposure dynamics were modelled across three operational scenarios.

Furthermore, the model exclusively tracks the growth and toxigenesis of the baseline *S. aureus* population present within the commercial package upon unsealing ($[\text{S.aureus}]_0$); potential secondary cross-contamination via manual handling or utensils during retail portioning was outside the quantitative scope of this exposure assessment.

2.3.1. Scenario 1 (S1): Commercial Semi-Open Display Counter Service

Scenario S1 simulates a commercial retail service where the opened matrix is displayed in refrigerated, open-top showcases. Because these display units lack a hermetic enclosure, the matrix is subject to vertical thermal stratification: Conductive cooling chills the bottom stainless-steel surface while ambient room air and lighting warm the upper surface layers.

Thermal variability in the showcase (T_{S1}) was parameterized from expert elicitation and verified by empirical retail survey data from 15 shops as a three-parameter PERT distribution:

$$T_{\text{S1}} \sim \text{PERT}\left(4^{\circ}\text{C},\ 12^{\circ}\text{C},\ 15^{\circ}\text{C}\right)$$

Active display duration during an individual meal service depends on the dining period (lunch or dinner). Elapsed holding and consumption time (t_{S1}), representing the cumulative interval from counter placement to ingestion, was parameterized separately for midday and evening services:

- Lunch service ($t_{\text{S1-lunch}}$): Modelled as $t_{\text{S1-lunch}} \sim \text{PERT}(0\ \text{h},\ 2.5\ \text{h},\ 4\ \text{h})$, corresponding to the product dispensed during the midday peak (10:00 AM to 2:00 PM).
- Dinner service ($t_{\text{S1-dinner}}$): Modelled as $t_{\text{S1-dinner}} \sim \text{PERT}(8\ \text{h},\ 10.5\ \text{h},\ 12\ \text{h})$, capturing extended counter holding when batches opened in the morning are served through late afternoon and evening until retail closing (10:00 PM).

2.3.2. Scenario 2 (S2): Room-temperature service across regions and seasons

Scenario S2 represents nonrefrigerated retail holding, where the product is held at room temperature without active mechanical chilling. Because indoor room temperatures $\left(T_{room,i,j}\right)$ vary substantially across territories and seasons, thermal conditions were parameterized by geographical region ($i = 1, \ldots, 7$) and season ($j = 1, \ldots, 4$):

$$T_{\text{room},i,j} \sim \text{Uniform}\left(T_{\text{med-min},i,j},\ T_{\text{med-max},i,j}\right)$$

where $T_{\text{med-min},i,j}$ and $T_{\text{med-max},i,j}$ denote the median of the daily minimum (T_{min}) and maximum (T_{max}) temperatures, respectively, compiled for region i($i = 1, \ldots, 7$) during season j($j = 1, \ldots, 4$) (for each season, temperatures were collected throughout all the corresponding months) (Table 1). This formulation captures the seasonal heat loads in retail spaces operating without continuous HVAC climate control.

The service schedules and exposure durations for Scenario S2 were set identically for lunch and dinner service.

$$t_{\text{S2}} \sim \text{PERT}(0\ \text{h},\ 2.5\ \text{h},\ 4\ \text{h})$$

.

2.3.3. Scenario 3 (S3): Leftover Storage and Delayed Consumption

Scenario S3 simulates the operational fate of unsold commercial counter meatballs or unconsumed leftovers originating from Scenarios S1 or S2. When food remains unsold, it is removed from the counter, rewrapped, and transferred to closed refrigeration ($T_{\text{cold}} \sim \text{Uniform}\left(4.0{,}8.0\,^{\circ}\text{C}\right)$) under one of two defined holding intervals (t_m) prior to delayed consumption: post-lunch leftover storage ($t_{\text{m-lunch}} = 8\text{h}$), where leftover meatballs from lunch service

undergo an interim cold-holding interval prior to secondary evening dispensing for the both scenarios S1 and S2, while post-dinner leftover storage ($t_{\text{m-dinner}} = 12\text{h}$), where unsold evening meatballs are held overnight in refrigeration prior to next-day consumption only for the S1.

Owing to limitations in the available data, this study focused solely on the probabilistic assessment of SE concentrations per meatball under each scenario, starting from a 10,000 g package unit. The model output is expressed as the predicted *S. aureus* concentration ($\log_{10}\text{CFU g}^{-1}$) and enterotoxin level (ng/meatball) at the time of consumption. Although a full exposure assessment would require data on consumption frequency, these data were excluded because of the lack of reliable consumer data. Although typical consumer intake ranges from one to eight hand-formed meatballs ($25\text{--}200\text{g}$ per meal), a single standardized meatball ($W_{\text{meatball}} = 25\text{g}$) was adopted as the reference unit mass to quantify per-meatball enterotoxin doses ($D_{\text{SE,meatball}}$, Eq. 12) and determine the minimum number of meatballs required to reach the acute intoxication threshold ($\text{meatballs}_{\text{min}}$, Eq. 14)

2.4. Literature Data Extraction and Parameterization of the Initial Contamination of *S. aureus*

To establish the initial contamination distribution ($S.\,\text{aureus}_0$) of *S. aureus*, a structured literature search was conducted across PubMed, Web of Science, and Google Scholar for studies evaluating retail *çiğ köfte* in Türkiye. The inclusion criteria included peer-reviewed empirical publications reporting quantitative enumeration data (CFUg^{-1}) alongside contamination frequencies. A total of 13 peer-reviewed articles met the initial screening criteria, of which 9 provided quantitative staphylococcal enumeration data (CFUg^{-1}) suitable for baseline concentration modelling (while the remaining 4 reported only qualitative prevalence or non-specific counts). Among these 9 quantitative studies, three reported aggregate *Micrococcus–Staphylococcus* counts, whereas six focused specifically on coagulase-positive staphylococci (CPS).

To reliably parameterize the stochastic exposure model, eligible datasets were evaluated on the basis of sample size (n), enumeration metrics, and distribution granularity. Among the six CPS studies, the empirical dataset published by Delikanlı et al. (2014) was selected as the reference baseline because it provided complete, discrete enumeration counts for each individual sample ($n = 30$). Furthermore, because 100% of the sampled units in this cohort were positive for coagulase-positive staphylococci, the baseline contamination model did not require zero inflation or external prevalence adjustment, permitting direct empirical sampling.

As summarized in Table 2, the initial concentration of *S. aureus* per commercial package ($[S.\ aureus]_{\text{package}}$, CFU/package) was modelled using Equations 1 and 2:

Table 2
Stochastic input parameters, probability distributions, and initial contamination of coagulase-positive staphylococci and *S. aureus* in commercial plant-based *çiğ köfte* packages.

Parameter	Symbol	Unit	Input	Mathematical/Stochastic Definition	Data Source
Coagulase-Positive Staphylococci	$[\text{CPS}]_0$	CFU g^{-1}	Empirical data $n = 30$, Prevalence $= 100\%$	$\text{DiscreteUniform}\left(\{N_1, \ldots, N_{30}\}\right)$	Delikanlı et al. (2014);
Species Attribution Fraction	$P_{S.\,aureus}$	Dimensionless	Assumption	$\text{Uniform}(0, 1)$	In this study
Initial *S. aureus* Concentration	$[S.\,aureus]_0$	CFU g^{-1}	Calculated	$P_{S.\,aureus} \times [\text{CPS}]_0$	Stochastic model output, in this study
Wholesale Package Net Weight	W_{package}	g	Standard commercial bulk packaging mass in Türkiye	Deterministic constant	In this study
Final package *S. aureus* concentration	$C_{\text{package}} \sim [S.\,aureus]_{\text{package}}$	CFU/package	Calculated	$[S.\,aureus]_0 \times W_{\text{package}}$	Stochastic model output, in this study

$[\text{CPS}]_0$, initial baseline concentration of coagulase-positive staphylococci sampled nonparametrically from discrete plate counts (N_1, N_2, ..., N_{30}) reported by Delikanlı et al. (2014);$P_{S.\,aureus}$, attribution ratio representing the proportion of confirmed *S. aureus* within isolated coagulase-positive staphylococci, modelled as a standard continuous uniform distribution Uniform(0, 1) to capture complete epistemic uncertainty in the absence of species-specific molecular typing;$[S.\,aureus]_0$, initial *S. aureus* concentration per gram of *çiğ köfte* prior to retail display, computed using Eq. 2; W_{package}, net weight of standard wholesale commercial bulk vacuum containers (10,000 g = 10 kg) distributed to retail outlets in Türkiye; $[S.\,aureus]_{\text{package}}$, total staphylococcal cell load per sealed bulk package at retail delivery prior to display opening (Eq. 1). CFU, colony-forming units.

$$C_{\text{package}} \sim [S.\,aureus]_{\text{package}} = [S.\,aureus]_0 \times W_{\text{package}} \quad \textbf{(Eq. 1)}$$

where:

- $[S.\ aureus]_0$: Initial concentration of *S. aureus* ($\mathrm{CFU\backslash:g^{-1}}$ofçiğköfte), estimated via Eq. 2;
- W_{package} : Net weight of a wholesale/retail commercial *çiğ köfte* container ($10{,}000$ g).

Because Delikanlı et al. (2014) enumerated total coagulase-positive staphylococci on selective Baird–Parker agar, a group that comprises *S. aureus* as well as other CPS species, the initial concentration of confirmed *S. aureus* was partitioned using a stochastic ratio:

$$[S.\ aureus]_0 = P_{S.\ aureus} \times [\mathrm{CPS}]_0 \quad \textbf{(Eq. 2)}$$

where:

- $[\mathrm{CPS}]_0$: Initial concentration of coagulase-positive staphylococci ($\mathrm{CFU\backslash:g^{-1}}$), sampled directly from the 30 individual empirical enumeration values reported by Delikanlı et al. (2014) using a discrete uniform distribution:

$$[\mathrm{CPS}]_0 \sim \mathrm{DiscreteUniform}\left(\left\{N_1, N_2, \ldots, N_{30}\right\}\right)$$

- $P_{S.\ aureus}$: Proportion of *S. aureus* within the isolated CPS population. In the absence of species-level molecular or phenotypic subtyping across raw retail isolates, complete epistemic uncertainty was assumed and represented by a uniform distribution:

$$P_{S.\ aureus} \sim \mathrm{Uniform}(0,\ 1)$$

2.5. Microbial challenge test

2.5.1. Bacterial strains

Owing to the absence of sufficient data on the growth dynamics of *S. aureus* in *çiğ köfte*, a controlled challenge test was conducted under laboratory conditions. For this purpose, *çiğ köfte* was aseptically prepared to closely replicate real-life conditions while minimizing external microbial interference. The experimental design followed the guidelines proposed by Russell and Gould (2003) and involved testing the growth potential of three available clinical reference strains of *S. aureus* (ATCC 43300, ATCC 29213, and D4508) in triplicate. These strains were selected to represent a broader phenotypic spectrum of *S. aureus* under identical food matrices and environmental conditions. ATCC 43300, a methicillin-resistant strain recommended by EUCAST for antimicrobial susceptibility testing, and ATCC 29213, a methicillin-sensitive quality control strain widely used in growth studies, were included to assess potential variability in growth kinetics and stress responses. In addition, strain D4508, which carries the sea gene and exhibits enterotoxigenic activity by producing staphylococcal enterotoxin A (SEA), was selected because of its enterotoxigenic potential, making it particularly relevant for food safety evaluations involving toxin production. We acknowledge that these are clinical reference strains and not foodborne isolates from outbreaks. However, their well-characterized growth behavior and toxin profiles enable standardized comparisons under controlled conditions, although this may limit direct extrapolation to field strains. The strains were individually inoculated into the *çiğ köfte* matrix, and their growth behavior was monitored to estimate relevant microbial growth parameters.

2.5.2. Preparation of çiğ köfte

A total of 1000 grams of fine brown bulgur was placed in a sterile stainless-steel tray. Afterward, 60 grams of tomato paste and 60 grams of pepper paste were added and mixed together. Approximately 30 grams of fresh garlic and 240 grams of finely blended onion were homogenized and incorporated into the mixture. Afterward, 150 grams of isot pepper (a unique sun-dried and fermented chili flake from Southeastern Anatolia, Türkiye), 250 mL of olive oil, juice from one lemon, and 50 mL of pomegranate molasses were added. Finally, 5 grams of black pepper and 5 grams of salt were introduced. The mixture was kneaded thoroughly by hand using sterile gloves, and approximately 250–300 mL of water was gradually added until the bulgur softened and reached the desired consistency. The kneading process lasted approximately 30 minutes until a homogeneous, dough-like structure was obtained. Although the product is traditionally artisanal and not subjected to heat processing, the mixture was sterilized in an autoclave at 121°C for 15 minutes following preparation. This step aimed to eliminate any preexisting microbial contamination and ensure that only the inoculated bacteria would be present without interference from the background microbiota. Physicochemical measurements confirmed that autoclaving did not significantly alter matrix properties ($p > 0.05$), with $\mathrm{pH} = 5.30 \pm 0.09$ and $a_w = 0.952 \pm 0.004$ before sterilization versus $\mathrm{pH} = 5.19 \pm 0.05$ and $a_w = 0.927 \pm 0.01$ after sterilization, and no perceptible changes were observed in physical or sensory characteristics. After sterilization, the *çiğ köfte* was cooled to room temperature and divided into 10 g meatballs, each placed into sterile filter bags.

2.5.3. Inoculation and enumeration of S. aureus in çiğ köfte

The bacterial precultures were prepared in tryptic soy broth (TSB) (Oxoid CM0129) and incubated at 37°C for 24 hours. The final inoculum volume was kept below 1% (v/w) to preserve the original sensory and physicochemical properties of the *çiğ köfte* matrix. This limitation also aimed to avoid excess moisture that could alter the texture of the product. As a result, the target inoculation level was approximately 4 $\log_{10}$ CFU $\mathrm{g^{-1}}$ for each *S. aureus* strain. A high inoculum level was chosen to prevent false-negative results due to growth inhibition or extended lag times in potentially stressed *S. aureus* cells. Following inoculation, the samples were transferred into sterile Stomacher blender bags and incubated at 22°C, with all experimental conditions performed in triplicate. Bacterial growth was monitored at 13 time points (0, 20 min, 40 min, 1 h, 1.5 h, 2 h, 3 h, 4 h, 6 h, 8 h, 12 h, 18 h, and 24 h). At each time point, one bag from each biological replicate (n = 3) was retrieved, and its content was serially diluted tenfold in sterile peptone water. The diluted samples were homogenized using a Stomacher blender, and 500 µL aliquots were plated onto Baird–Parker agar (Oxoid CM0275) supplemented with an egg yolk tellurite emulsion (Oxoid SR0054). A 500 µL aliquot volume was chosen to increase the analytical sensitivity and achieve a lower limit of detection. The plates were incubated at 37°C for 24–48 hours.

2.6. Modelling of *S. aureus* Growth

2.6.1. Bacterial Growth Primary Kinetic Parameter Estimation

Primary growth curves for each biological replicate ($n = 3$ per strain, yielding 9 independent curves) were fitted using the Baranyi and Roberts primary model implemented in the predictive microbiology platform Sym'Previus (v3.2.0; Sym'Previus, France; https://symprevius.eu/) to estimate the lag time ($\lambda_{22\,^\circ\mathrm{C}}$, h), the maximum specific growth rate ($\mu_{22\,^\circ\mathrm{C}}$, h^{-1}), and the maximum population density ($[S.\ aureus]_{\max}$, $\log_{10}\mathrm{CFU}\cdot\mathrm{g}^{-1}$). Goodness-of-fit was assessed using the residual sum of squares (RSS).

2.6.2. Estimation of the Optimum Growth Rate (μ_{opt}) and Secondary Modelling

To model bacterial growth across all the studied scenarios, the optimum specific growth rate (μ_{opt}) in the plant-based *çiğ köfte* matrix was determined using the Gamma (γ) concept (Koutsoumanis, 2001; Rosso et al., 1993):

$$\mu_{\mathrm{opt}} = \frac{\mu_{22\,^\circ\mathrm{C}}}{\gamma\left(22\,^\circ\mathrm{C}\right)} \quad \textbf{(Eq. 3)}$$

where:

- μ_{opt} : Optimum specific growth rate (h^{-1}) in the formulated *çiğ köfte* matrix when $T = T_{\mathrm{opt}}$;.
- $\mu_{22\,^\circ\mathrm{C}}$: Maximum specific growth rate (h^{-1}) derived from the empirical challenge tests at 22°C. Rather than using a single point estimate, biological variability across strains and replicates was explicitly incorporated by resampling equiprobably across all $k = 9$ primary model estimates (Table 5) using a discrete uniform distribution:

Table 5
Fitted primary growth parameters (± SE) of *S. aureus* strains in *çiğ köfte* at 22°C.

Strain/Source	Biological Replicate	Lag time $\lambda_{22°C}$ (h)	Specific Growth Rate $\mu_{22°C}$ (h^{-1})	$[S.\ aureus]_{max}$ log_{10}CFU g^{-1}	RSS
ATCC 29213	Rep 1	0.00	0.072 ± 0.05	5.30 ± 0.41	0.107
	Rep 2	0.29 ± 0.17	0.829 ± 0.19	4.92 ± 0.63	0.041
	Rep 3	3.28 ± 1.73	0.033 ± 0.01	5.75 ± 1.21	0.100
D4508	Rep 1	6.43 ± 0.72	0.192 ± 0.01	5.65 ± 0.43	0.088
	Rep 2	2.47 ± 0.41	0.330 ± 0.09	6.58 ± 0.12	0.119
	Rep 3	1.85 ± 0.02	1.010 ± 0.02	7.31 ± 0.62	0.013
ATCC 43300	Rep 1	11.66 ± 0.28	0.365 ± 0.02	4.49 ± 0.09	0.092
	Rep 2	2.86 ± 1.88	0.080 ± 0.02	4.20 ± 0.79	0.152
	Rep 3	0.00	0.120 ± 0.30	5.75 ± 0.56	0.060

λ_{22}, lag time (h) at 22°C; $\mu_{22\,^\circ\mathrm{C}}$, maximum specific growth rate at 22°C (h^{-1}); $[S.\ aureus]_{\max}$, maximum population concentration ($\log_{10}\mathrm{CFU}\,\mathrm{g}^{-1}$); Rep 1–Rep 3, independent biological replicates ($\mathrm{n} = 3$); RSS, residual sum of squares of the primary model fit.

$$\mu_{22\,^\circ\mathrm{C}} \sim \mathrm{DiscreteUniform}\left(\left\{\mu_{1,22\,^\circ\mathrm{C}}, \cdots, \mu_{9,22\,^\circ\mathrm{C}}\right\}\right)$$

- $\gamma\,(22°\mathrm{C})$: Dimensionless environmental factor ($0 \leq \gamma \leq 1$) quantifying the fractional reduction in the growth rate at 22°C relative to the optimum temperature ($T_{\mathrm{opt}} = 37\,^\circ\mathrm{C}$).

The value $\gamma\,(T)$ was calculated using the Cardinal Temperature Model with Inflection (CTMI) proposed by Rosso et al. (1993):

$$\gamma\,(T) = \begin{cases} 0, & \text{if} T < T_{\min} \text{or} T > T_{\max} \\ \dfrac{\left(T - T_{\min}\right)^2 \left(T - T_{\max}\right)}{\left(T_{\mathrm{opt}} - T_{\min}\right)\left[\left(T_{\mathrm{opt}} - T_{\min}\right)\left(T - T_{\mathrm{opt}}\right) - \left(T_{\mathrm{opt}} - T_{\max}\right)\left(T_{\mathrm{opt}} + T_{\min} - 2T\right)\right]}, & \text{if} T_{\min} \leq T \leq T_{\max} \end{cases} \quad \textbf{(Eq. 4)}$$

The cardinal temperature parameters were defined on the basis of published values for *S. aureus* reported in Table 3 published by Ziane & Membré (2022):

Table 3
Literature-derived minimum ($T_{\min}$) and maximum ($T_{\max}$) cardinal temperatures for *S. aureus* growth.

Reference	T_{min} (°C)	T_{max} (°C)
Angelotti et al. (1961)	6.5	45.6
Baeza et al. (2009)	7.0	48.0
Choi et al. (2019)	3.3–10.0	NR
De Matos (2013)	10.0	45.0
FDA (2012)	7.0	47.8
ICMSF (1996)	7.0	48.0
Kadariya et al. (2014)	7.0	48.5
Kang et al. (2013)	7.0	48.0
Le Loir et al. (2003)	10.0	48.0
Medveďová & Valík (2012)	7.0–8.0	46.0
Martin & Iandolo (2000)	7.0–8.0	NR
Missiakas & Schneewind (2013)	10.0	42.0
Schmitt et al. (1990)	7.0	48.5
Wang et al. (2017)	5.0–10.0	NR
Parametric Bound Range	[6.5–10.0]	[42.0–48.5]

NR = not reported. The values in the parametric bound range define the lower and upper limits of the continuous uniform prior distributions implemented in the exposure assessment: $T_{\min} \sim \text{Uniform}\left(6.5, 10.0\,^{\circ}\text{C}\right)$ and $T_{\max} \sim \text{Uniform}\left(42.0, 48.5\,^{\circ}\text{C}\right)$

- T_{opt} : Optimum growth temperature, set deterministically at 37°C.
- $T_{\min}$: Theoretical minimum growth temperature below which $\gamma(T) = 0$, parameterized as a uniform distribution across the literature bounds (Table 3) to account for strain-dependent physiological variability: $T_{\min} \sim \text{Uniform}\left(6.5, 10.0\,^{\circ}\text{C}\right)$;
- $T_{\max}$: Theoretical maximum growth temperature above which $\gamma(T) = 0$, parameterized as a continuous uniform distribution across the literature bounds (Table 3) to account for strain-dependent physiological variability: $T_{\max} \sim \text{Uniform}\left(42.0\,^{\circ}C, 48.5\,^{\circ}\text{C}\right)$.

By propagating these cardinal temperature distributions alongside empirical $\mu_{22\,^{\circ}\text{C}}$ values through Monte Carlo simulation (10^6 iterations in @RISK), μ_{opt} was obtained as an empirical probability density function, capturing both biological heterogeneity and parametric uncertainty in the quantitative microbial exposure assessment.

2.6.3. Estimation of S. aureus Growth Parameters under Different Temperature Scenarios

The growth parameters (μ_T and λ_T) across the defined temperature scenarios (S_1, S_2 and S_3) were determined using Equations 05 and 06 on the basis of the gamma concept and the work-to-be-done hypothesis (Koutsoumanis, 2001) (Table 4).

Table 4

Stochastic parameterization, environmental conditions, and predictive mathematical framework of *Staphylococcus aureus* growth dynamics and enterotoxi

Exposure Pathway & Stage	Description	Holding Temperature (T, °C)	Duration (t, h)	Kinetic Parameters & Probabilities
Retail Cold Storage (Before Opening)	Bulk-packaged inventory stored under wholesale/retail refrigeration	$T_{\text{cold}} \sim \text{Uniform}(4.0,8.0)$	$t_{\text{cold}} = 96.0$	μ_{cold}[Eq. 5]; λ_{cold}[Eq. 6]; $P_{\text{cold}}^{\text{no_lag}} = \text{RiskTarg}$
Lunch Service (S1)	Semi-open refrigerated showcase during midday peak	$T_{S1} \sim \text{PERT}(4.0,12.0,15.0)$	$t_{\text{S1-lunch}} \sim \text{PERT}(0.0,2.5,4.0)$	μ_{S1}[Eq. 5];λ_{S1}[Eq. 6]; $P_{\text{cold}}^{\text{no_lag}}$(entry); $P_{\text{S1-lunch}}^{\text{no_lag}} = \text{RiskTar}$ (exit)
Dinner Service (S1)	Extended showcase display until retail closing	$T_{S1} \sim \text{PERT}(4.0,12.0,15.0)$	$t_{\text{S1-dinner}} \sim \text{PERT}(8.0,10.5,12.0)$	μ_{S1}[Eq. 5];λ_{S1}[Eq. 6]; $P_{\text{cold}}^{\text{no_lag}}$(entry); $P_{\text{S1-dinner}}^{\text{no_lag}} = \text{RiskTa}$ (exit)
Post-Lunch Leftovers (S3 ex-S1)	Unsold lunch counter meatballs returned to closed refrigeration	$T_{\text{cold}} \sim \text{Uniform}(4.0,8.0)$	$t_{\text{m-lunch}} = 8.0$	μ_{cold}[Eq. 5]; λ_{cold}[Eq. 6]; $P_{\text{S1-lunch}}^{\text{no_lag}}$(entry)
Post-Dinner Leftovers (S3 ex-S1)	Overnight closed refrigeration of unsold dinner counter meatballs	$T_{\text{cold}} \sim \text{Uniform}(4.0,8.0)$	$t_{\text{m-dinner}} = 12.0$	μ_{cold}[Eq. 5]; λ_{cold}[Eq. 6]; $P_{\text{S1-dinner}}^{\text{no_lag}}$(entry)
Lunch/Dinner Service (S2)	Unrefrigerated room display across 7 regions (*i*) and 4 seasons (*j*)	$T_{\text{room},i,j} \sim \text{Uniform}\left(T_{\text{med-min},i,j}, T_{\text{med-max},i,j}\right)$ (Table 1)	$t_{S2} \sim \text{PERT}(0.0,2.5,4.0)$	$\mu_{S2,i,j}$[Eq. 5];$\lambda_{S2,i,j}$ $P_{\text{cold}}^{\text{no_lag}}$(entry); $P_{S2,i,j}^{\text{no_lag}} = \text{RiskTarg}$
Post-Lunch Leftovers (S3 ex-S2)	Unsold ambient lunch meatballs transferred to closed refrigeration	$T_{\text{cold}} \sim \text{Uniform}(4.0,8.0)$	$t_{\text{m-lunch}} = 8.0$	μ_{cold}[Eq. 5]; λ_{cold}[Eq. 6]; $P_{S2,i,j}^{\text{no_lag}}$(entry)

* The enterotoxigenic *S. aureus* concentration ($C_{\text{stage}}^{\text{comp_ent}}$, **Eq. 10**) was estimated from the predicted composite *S. aureus* concentration ($C_{\text{stage}}^{\text{comp}}$) and the er primary empirical toxigenesis model (**Eq. 11**) to estimate staphylococcal enterotoxin levels (SE_{stage}).

$\mu_T = \gamma(T) \times \mu_{\text{opt}}$ **(Eq. 5)**

where:

- μ_T: specific growth rate (h^{-1}) under a given temperature scenario (T_{S1}, $T_{\text{room},i,j}$, or T_{cold});
- $\gamma(T)$: temperature-dependent gamma function value (Eq. 4);
- μ_{opt} : maximum specific growth rate (h^{-1}) under optimal conditions (Eq. 3).

For room temperature scenarios, $T_{room,i,j}$ values were modelled using a continuous uniform distribution (see section 2.3.2.).

The lag time (λ_T) was estimated according to Eq. 6:

$$\lambda_T = \begin{cases} \frac{\mu_{22\,^\circ\mathrm{C}} \times \lambda_{22\,^\circ\mathrm{C}}}{\mu_T}, & \text{if } T > T_{\min} \\ \infty, & \text{if } T \le T_{\min} \end{cases} \quad \textbf{(Eq. 6)}$$

where λ_T is the lag time (h) in a given temperature scenario (T_{S1}, $T_{room,i,j}$ or T_{cold}), and $\mu_{22\,^\circ\mathrm{C}}$ and $\lambda_{22\,^\circ\mathrm{C}}$ represent the growth parameters calculated at $22\,^\circ\mathrm{C}$.

2.6.4. Modelling Lag Phase Transitions and the No-Lag State ($P^{\mathrm{no_lag}}$)

The bacterial cells were assumed to be in an unstressed, physiologically active state at the beginning of the next scenario (S1, S2, or S3). In the Monte Carlo simulation executed in @RISK (Palisade Corporation, Ithaca, NY, USA), lag phase progression across sequential supply chain stages was quantified via cumulative state-transition probabilities rather than resetting the lag phase at each stage boundary:

- **Initial wholesale and retail cold holding ($T_{\mathrm{cold}} \sim \mathrm{Uniform}\left(4.0\,^\circ\mathrm{C}, 8.0\,^\circ\mathrm{C}\right)$, $t_{\mathrm{cold}} = 96.0\mathrm{h}$)**: The probability of fully exhausting the pre-display lag time within the 96.0 h cold-storage window was evaluated using the cumulative distribution function:

$$P_{\mathrm{cold}}^{\mathrm{no_lag}} = \mathrm{RiskTarget}\left(\lambda_{\mathrm{cold}}, 96.0\right)$$

which represents the proportion of simulated cold-storage states in which $\lambda_{\mathrm{cold}} \le 96.0\mathrm{h}$ prior to package opening.

- **Transition to commercial retail display (Scenarios S1 and S2)**: Subpopulations that resolved their lag phase during pre-opening cold storage entered retail display ready for immediate exponential division ($\lambda_{S1} = 0\mathrm{h}$ and $\lambda_{S2,i,j} = 0\mathrm{h}$) with probability weight $P_{\mathrm{cold}}^{\mathrm{no_lag}}$, whereas the remaining fraction $\left(1 - P_{\mathrm{cold}}^{\mathrm{no_lag}}\right)$ retained its temperature-dependent display lag phase (λ_{S1} or $\lambda_{S2,i,j}$).
- **Transition to refrigerated leftover storage (Scenario S3)**: For unsold meatballs returned to closed refrigeration ($T_{\mathrm{cold}} \sim \mathrm{Uniform}\left(4.0\,^\circ\mathrm{C}, 8.0\,^\circ\mathrm{C}\right)$) following lunch ($t_{S1\text{-lunch}}$ or $t_{S2} \sim \mathrm{PERT}(0.0\mathrm{h}, 2.5\mathrm{h}, 4.0\mathrm{h})$) or dinner ($t_{S1\text{-dinner}} \sim \mathrm{PERT}(8.0\mathrm{h}, 10.5\mathrm{h}, 12.0\mathrm{h})$) display, the probability weight for immediate proliferation without a residual cold-storage lag phase ($\lambda_{\mathrm{cold}} = 0\mathrm{h}$) was evaluated according to the preceding service window:

$$P_{S1\text{-meal}}^{\mathrm{no_lag}} = \mathrm{RiskTarget}\left(\lambda_{S1}, t_{S1\text{-meal}}\right) \quad \text{and} \quad P_{S2,i,j}^{\mathrm{no_lag}} = \mathrm{RiskTarget}\left(\lambda_{S2,i,j}, t_{S2}\right)$$

These transition functions quantify the probability that the lag phase was already completed ($\lambda \le t$) during the preceding counter display (S1) or room-temperature holding (S2), while the complementary fraction— $\left(1 - P_{S1\text{-meal}}^{\mathrm{no_lag}}\right)$ and $\left(1 - P_{S2,i,j}^{\mathrm{no_lag}}\right)$, respectively—entered leftover refrigeration retaining a residual lag phase.

2.6.5. Estimation of S. aureus concentrations at each serving stage

To integrate primary exponential growth kinetics (Nauta et al., 2003) with sequential lag-phase state transitions without introducing discrete Bernoulli discontinuities across Latin hypercube iterations, the bacterial concentration at serving time was formulated as a probability-weighted composite log-concentration ($C_{\mathrm{stage}}^{\mathrm{comp}}$, $\log_{10}\mathrm{CFU} \cdot \mathrm{g}^{-1}$) across each retail and leftover stage (Eq. 7; Table 4):

$$C_{\mathrm{stage}}^{\mathrm{comp}} = P_{\mathrm{stage}}^{\mathrm{no_lag}} \times C^{\mathrm{no_lag}} + \left(1 - P_{\mathrm{stage}}^{\mathrm{no_lag}}\right) \times C^{\mathrm{lag}} \quad \textbf{Eq. 7}$$

where $C^{\mathrm{no_lag}}$ (Eq. 8) and C^{lag} (Eq. 9) represent the conditional bacterial concentrations ($\log_{10}\mathrm{CFU} \cdot \mathrm{g}^{-1}$) achieved with an exhausted lag phase ($\lambda_T = 0$) and with a full temperature-dependent lag phase ($\lambda_T > 0$), respectively:

$$C_{\mathrm{no_lag}} = \min\left([S.\,\mathrm{aureus}]_{\max}, [S.\,\mathrm{aureus}]_{\mathrm{initial}} + \mu_T \cdot t_T\right) \quad \textbf{Eq. 8}$$

$$C_{\mathrm{lag}} = \begin{cases} [S.\,\mathrm{aureus}]_{\mathrm{initial}}, & \text{for } t_T \le \lambda_T \\ \min\left([S.\,\mathrm{aureus}]_{\max}, [S.\,\mathrm{aureus}]_{\mathrm{initial}} + \mu_T\left(t_T - \lambda_T\right)\right), & \text{for } t_T > \lambda_T \end{cases} \quad \textbf{Eq. 9}$$

Structurally, Eq. 7 computes the expected $\log_{10}$ cell density across the two physiological states (corresponding to a probability-weighted geometric mean of the lag-resolved and lag-retaining subpopulations), thereby ensuring smooth variance propagation across all 10^6 Monte Carlo iterations.

where:

- $C_{\mathrm{stage}}^{\mathrm{comp}}$ is the composite *S. aureus* population concentration ($\log_{10}\mathrm{CFU} \cdot \mathrm{g}^{-1}$) predicted at the point of retail dispensing or delayed consumption across operational scenarios ($C_{\mathrm{lunch},S1}^{\mathrm{comp}}$, $C_{\mathrm{dinner},S1}^{\mathrm{comp}}$, $C_{S2,i,j}^{\mathrm{comp}}$, or downstream refrigerated leftover concentrations $C_{\mathrm{leftover}}^{\mathrm{comp}}$, as detailed in Table 4);

- $P_{\text{stage}}^{\text{no_lag}}$ is the discrete transition probability at which bacterial cells enter the designated stage with an already exhausted lag time ($P_{\text{cold}}^{\text{no_lag}}$, $P_{S1\text{-meal}}^{\text{no_lag}}$, or $P_{S2,i,j}^{\text{no_lag}}$), weighting the subpopulation undergoing instantaneous division ($C_{\text{no_lag}}$) against that retaining residual lag phase ($1 - P_{\text{stage}}^{\text{no_lag}}$) (Section 2.6.4; Table 4);
- $[S.\,\text{aureus}]_{\text{initial}}$ is the baseline concentration ($\log_{10}\text{CFU} \cdot \text{g}^{-1}$) entering the operational phase. For retail display (Scenarios S1 and S2), $[S.\,\text{aureus}]_{\text{initial}}$ corresponds to the unsealed container concentration ($[S.\,\text{aureus}]_0$, Eq. 2); for secondary leftover refrigeration (Scenario S3), $[S.\,\text{aureus}]_{\text{initial}}$ was initialized from the terminal concentration reached at the end of the preceding display period (S1 or S2);
- μ_T is the maximum specific growth rate (h^{-1}) at holding temperature T(°C), computed via the secondary cardinal model (Eq. 5);
- t_T is the operational elapsed holding duration (h) parameterized according to the service window or leftover storage scenario (e.g., t_{lunch}, t_{dinner}, or t_{S2}; Table 4);
- λ_T is the temperature-dependent lag phase duration (h) under holding temperature T(°C), derived from the work-to-be-done hypothesis (Eq. 6);
- $[S.\,\text{aureus}]_{\max}$ denotes the upper carrying capacity supported by the plant-based matrix ($\log_{10}\text{CFU} \cdot \text{g}^{-1}$), parameterized at the upper standard error bound of $7.93\log_{10}\text{CFU} \cdot \text{g}^{-1}$ ($7.31 + 0.62\log_{10}\text{CFU} \cdot \text{g}^{-1}$) on the basis of empirical stationary-phase counts observed in strain D4508 (Rep 3), representing a conservative, health-protective worst-case scenario (Table 5).

2.6.6. Probability of critical staphylococcal enterotoxin concentrations

Enterotoxin production is conditioned upon reaching a critical bacterial concentration of $5.0\log_{10}\text{CFUg}^{-1}$ (Kim et al., 2009). Staphylococcal enterotoxin (SE) synthesis was considered negligible below this cell density ($SE_{\text{stage}} = 0$). To account for strain-level toxigenic heterogeneity, the enterotoxigenic *S. aureus* concentration ($C_{\text{stage}}^{\text{comp_ent}}$, $\log_{10}\text{CFUg}^{-1}$) was estimated at each stage from the predicted composite *S. aureus* concentration ($C_{\text{stage}}^{\text{comp}}$, **Eq. 7**) and the enterotoxigenic strain prevalence (P_{ET}), which was assigned a uniform prior distribution ($P_{\text{ET}} \sim \text{Uniform}(0,1)$) to reflect epistemic uncertainty (**Eq. 10**):

$$C_{\text{stage}}^{\text{comp_ent}} = P_{\text{ET}} \times C_{\text{stage}}^{\text{comp}} \quad \textbf{(Eq. 10)}$$

For enterotoxigenic populations meeting or exceeding the critical threshold ($C_{\text{stage}}^{\text{comp_ent}} \geq 5.0\log_{10}\text{CFUg}^{-1}$), staphylococcal enterotoxin accumulation was estimated using the primary empirical toxigenesis model formulated in **Eq. 11**:

$$SE_{\text{stage}} = \begin{cases} 0, & \text{if } C_{\text{stage}}^{\text{comp_ent}} < 5.0\log_{10}\text{CFUg}^{-1} \\ 10^{0.9301 \times C_{\text{stage}}^{\text{comp_ent}} - 6.6621}, & \text{if } C_{\text{stage}}^{\text{comp_ent}} \geq 5.0\log_{10}\text{CFUg}^{-1} \end{cases} \quad \textbf{(Eq. 11)}$$

where SE_{stage} is the predicted staphylococcal enterotoxin concentration (ngg^{-1} of çiğ köfte) and $C_{\text{stage}}^{\text{comp_ent}}$ is the enterotoxigenic bacterial concentration ($\log_{10}\text{CFUg}^{-1}$) at the end of each stage.

The total enterotoxin dose ($D_{\text{SE,meatball}}$, in ng) within a single 25g meatball was calculated via Eq. 12:

$$D_{\text{SE,meatball}} = [\text{SE}] \times W_{\text{meatball}} \quad \textbf{(Eq. 12)}$$

The probability that a single meatball exceeds a critical toxic threshold dose (CD) was evaluated as follows:

$$P_{\text{SE,meatball}} = P\left(D_{\text{SE,meatball}} > CD\right) = 1 - F_{D_{\text{SE}}}(CD) \quad \textbf{(Eq. 13)}$$

where CD represents the critical toxic dose, established at 100ng for sensitive populations. In @RISK, Eq. 13 is computed as $1 - RiskTarget(D_{\text{SE,meatball}}; CD)$.

Finally, the minimum number of meatballs ($\text{meatballs}_{\min}$) required to deliver a toxic dose under maximum enterotoxin accumulation ($D_{\text{SE,max}}$) was determined using the Eq. 14:

$$\text{meatballs}_{\min} = \lceil \frac{CD}{D_{\text{SE,max}}} \rceil \quad \textbf{(Eq. 14)}$$

2.7. Statistical Analysis and Outlier Detection

Interstrain differences in primary kinetic parameters (λ and $\mu_{\max}$) were evaluated using the nonparametric Kruskal–Wallis test, chosen because of the small sample size per group ($n = 3$). The consistency among the three biological replicates within each strain was screened for anomalous values using Grubbs' test at a significance threshold of $\alpha = 0.05$. When an outlier was detected, data points were not automatically eliminated; instead, a leave-one-out sensitivity analysis was conducted by fitting the primary growth model and comparing parameter estimates with and without the high-leverage replicate observation.

2.8. Monte Carlo Simulation and Sensitivity Analysis

Probabilistic modelling and quantitative exposure simulations were conducted using @RISK software (version 5.3.1; Palisade Corporation, Ithaca, NY, USA) implemented as an add-in for Microsoft Excel. To ensure representative coverage of the input parameter distributions and tail-end extreme events, a Monte Carlo simulation was executed with 10^6 iterations using Latin hypercube sampling (LHS) with a fixed random seed to ensure reproducibility. Convergence was verified by monitoring stability across the mean and upper percentiles (95th and 99th) of the primary output distributions.

A global sensitivity analysis was conducted to quantify the relative influence of stochastic input parameters (e.g., storage temperature, duration, initial contamination level, and enterotoxigenic prevalence) on the primary model endpoints: the final concentration of *S. aureus* ($\log_{10}\!:\mathrm{CFU}\!:\mathrm{g}^{-1}$) and the resulting staphylococcal enterotoxin dose ($D_{\mathrm{SE},\!:\mathrm{meatball}}$) in *çiğ köfte*. The relative contribution of each parameter was evaluated using Spearman's rank order correlation coefficients (r_s).

The overall modelling framework, including the exposure pathways, baseline variables, assigned probability density functions, and their respective literature sources, is summarized in Table 4.

3. RESULTS

3.1. Initial Contamination Distribution and *S. aureus* Load in *Çiğ köfte*

Initial contamination of *S. aureus* was parameterized using retail contamination data from Delikanlı et al. (2014), who provided discrete enumeration counts of coagulase-positive staphylococci (CPS) across 30 commercial plant-based *çiğ köfte* samples ($n = 30$). In that survey, CPS was detected in 100% of the tested units, yielding an empirical median concentration [CPS] of $2.57\ \log_{10}\!:\mathrm{CFU}\!:\mathrm{g}^{-1}$ ($\approx 3.7 \times 10^2\!:\mathrm{CFU}\!:\mathrm{g}^{-1}$) and a maximum observed concentration of $3.71\ \log_{10}\!:\mathrm{CFU}\!:\mathrm{g}^{-1}$ ($5.13 \times 10^3\!:\mathrm{CFU}\!:\mathrm{g}^{-1}$). Because individual plate counts were reported, initial CPS contamination was modelled nonparametrically using a discrete uniform distribution, which preserved empirical heterogeneity without imposing arbitrary parametric distribution assumptions. To account for epistemic uncertainty regarding the exact proportion of *S. aureus* within the CPS isolates, a standard uniform attribution prior was applied ($P_{S.\ aureus} \sim \mathrm{Uniform}(0,\ 1)$).

Propagating this baseline model through 10^6 Monte Carlo iterations for wholesale packages ($W_{\mathrm{package}} = 10{,}000\mathrm{g}$) resulted in an initial *S. aureus* package load with a median of $6.27\ \log_{10}\mathrm{CFU/package}$ ($\approx 1.86 \times 10^6\mathrm{CFU/package}$), a 95th percentile of $7.29\ \log_{10}\mathrm{CFU/package}$ ($\approx 1.95 \times 10^7\mathrm{CFU/package}$), and a maximum of $7.71\ \log_{10}\mathrm{CFU/package}$ ($\approx 5.13 \times 10^7\mathrm{CFU/package}$). On a per-gram of *çiğ köfte*, this translated to a median concentration of $2.27\ \log_{10}\!:\mathrm{CFU}\!:\mathrm{g}^{-1}$ ($\approx 1.86 \times 10^2\!:\mathrm{CFU}\!:\mathrm{g}^{-1}$), a 95th percentile of $3.29\ \log_{10}\!:\mathrm{CFU}\!:\mathrm{g}^{-1}$ ($\approx 1.95 \times 10^3\!:\mathrm{CFU}\!:\mathrm{g}^{-1}$), and a maximum initial concentration of $3.71\ \log_{10}\!:\mathrm{CFU}\!:\mathrm{g}^{-1}$ ($\approx 5.13 \times 10^3\!:\mathrm{CFU}\!:\mathrm{g}^{-1}$).

3.2. Estimation of Growth Parameters at 22°C

Primary growth curve modelling of the challenge test data ($n = 3$ independent biological replicates per strain) revealed substantial dispersion in both the lag time ($\lambda_{22°\mathrm{C}}$) and maximum specific growth rate ($\mu_{\max,22°\mathrm{C}}$) across the tested *S. aureus* strains (Table 5). Nonparametric Kruskal–Wallis testing detected no statistically significant interstrain differences for either lag duration ($p = 0.661$) or specific growth rate ($p = 0.393$), indicating that within the limited statistical power of the triplicate design ($n = 3$), replicate-to-replicate dispersion within the heterogeneous solid matrix exceeded interstrain divergence.

To account for the microenvironmental heterogeneity and experimental stochasticity inherent to the *çiğ köfte* matrix, the stability of the intrastrain kinetic parameters was evaluated via a leave-one-out sensitivity analysis. For strain ATCC 29213, $\lambda_{22\circ\mathrm{C}}$ ranged from 0.00 to 3.28 h and $\mu_{22\circ\mathrm{C}}$ ranged from 0.033 to 0.829 h⁻¹; iterative exclusion revealed a high-leverage replicate (3.28 h) that significantly skewed the estimated mean lag time (p = 0.029). Strain D4508 exhibited the highest overall kinetic activity, with $\mu_{22\circ\mathrm{C}}$ values ranging from 0.192 to 1.010 h⁻¹ and $\lambda_{22\circ\mathrm{C}}$ values ranging from 1.85 to 6.43 h, showing moderate sensitivity of the estimated lag time ($\lambda_{22\circ\mathrm{C}}$) to outlying observations (p = 0.046). Conversely, strain ATCC 43300 exhibited the most resilient kinetic profile ($\mu_{22\circ\mathrm{C}}$ = 0.080–0.365 h⁻¹; $\lambda_{22\circ\mathrm{C}}$ = 0.00–11.66 h), maintaining statistically consistent lag time ($\lambda_{22\circ\mathrm{C}}$) estimates against single-replicate perturbations regardless of whether the uppermost replicate (11.66 h) was retained (p = 0.08) or excluded (p = 0.35).

3.3. Estimation of *S. aureus* Growth and Enterotoxin Production under Different Temperature Scenarios

Stochastic simulations were used to quantify *S. aureus* growth dynamics and associated enterotoxin (SE) production across the three exposure scenarios. Because Scenario 3 (S3: leftover refrigeration) represents a dependent downstream stage parameterized by the final bacterial concentration and no lag time of the preceding retail display, its predictive outcomes are integrated directly into the evaluation of each respective scenario: Scenario S1 (counter display) and Scenario S2 (room display).

3.3.1. Scenario 1 ($\varvec{S_1}$): Commercial Semi-Open Display Counter Service

Stochastic simulation outputs indicated that display counter conditions occasionally permit the initiation of active staphylococcal proliferation. During the preceding refrigerated storage phase ($T_{\mathrm{cold}} \sim \mathrm{Uniform}\left(4.0,\ 8.0\ ^\circ\mathrm{C}\right)$, $t_{\mathrm{cold}} = 96.0\ \mathrm{h}$, prior to package unsealing), the cumulative probability of fully exhausting lag phase was 12.0% ($P_{\mathrm{cold}}^{\mathrm{no_lag}} = \mathrm{P}\left(\lambda_{\mathrm{cold}} \le 96.0\ \mathrm{h}\right) = \mathrm{RiskTarget}\left(\lambda_{\mathrm{cold}},\ 96.0\right) = 0.120$). Consequently, 12.0% of the retail display

iterations entered active log-linear replication immediately upon unsealing ($\lambda_{S1} = 0\ \mathrm{h}$), whereas the remaining $88.0\ \%$ remained subject to the display counter lag phase distribution (λ_{S1}). Within this display regime, 20.5% of iterations exhibited zero lag time (λ_{S1} = 0 h).

The specific growth rate under display counter conditions (T_{S1}) ranged from $0.000\mathrm{h}^{-1}$ to $0.461\mathrm{h}^{-1}$ (median: $0.016\mathrm{h}^{-1}$; 99th percentile: $0.267\mathrm{h}^{-1}$). During the lunch serving period ($t_{\mathrm{S1\text{-}lunch}} \sim \mathrm{PERT}(0\mathrm{h}, 2.5\mathrm{h}, 4\mathrm{h})$), bacterial concentration remained below the toxigenic threshold across all iterations, reaching an upper maximum of $3.85\log_{10}\mathrm{CFUg}^{-1}$ (median: $2.29\log_{10}\mathrm{CFUg}^{-1}$; 95th percentile: $3.42\log_{10}\mathrm{CFUg}^{-1}$).

During extended display through dinner service ($t_{\mathrm{S1\text{-}dinner}} \sim \mathrm{PERT}(8\ \mathrm{h},\ 10.5\ \mathrm{h},\ 12\ \mathrm{h})$), extreme tail iterations reached a maximum of $5.08\ \log_{10}\mathrm{CFU\,g}^{-1}$, exceeding the $5.0\log_{10}\mathrm{CFU\,g}^{-1}$ critical threshold with an exceedance probability of $P\left(C^{\mathrm{comp}}_{\mathrm{dinner,S1}} \geq\ 5.0\log_{10}\mathrm{CFU\,g}^{-1}\right) = 8.65 \times\ 10^{-3}$ (0.00865 of iterations). Despite these upper-tail threshold exceedances, toxigenic exposure remained negligible: because cell densities exceeded $5.0\log_{10}\mathrm{CFU\,g}^{-1}$ only marginally and for brief intervals, the maximum predicted enterotoxin accumulation in Scenario S1 was 1 ng per meatball. Reaching the toxicological illness threshold of 100 ng per meatball would thus require an unrealistic acute consumption of at least 100 individual meatballs.

Regarding residual lag phase progression during display, $27.5\ \%$ ($P^{\mathrm{no_lag}}_{S_1-lunch} = 0.275$) and $32.1\ \%$ ($P^{\mathrm{no_lag}}_{S_1-dinner} = 0.321$) exhibited lag phase durations shorter than the 4.0 h lunch and 12.0 h dinner service intervals, respectively. For these iterations, residual lag times were fully exhausted (set to λ = 0 h) upon transferring unsold meatballs to Scenario S3 (leftover domestic refrigeration at T_{cold}). Under Scenario S3 conditions, the maximum predicted concentrations reached $5.90\ \log_{10}\mathrm{CFU}g^{-1}$ (post-lunch) and $6.93\log_{10}\mathrm{CFU}g^{-1}$ (post-dinner), with $3.0\ \times\ 10^{-4}$ and $1.42\ \times\ 10^{-2}$ of meatballs exceeding the 5.0 $\log_{10}\mathrm{CFU}g^{-1}$ threshold, respectively (Table 6). Consequently, predicted enterotoxin accumulation across the entire simulation ensemble remained negligible, peaking at an upper-bound maximum of 2 ng per meatball. Given the widely established critical dose of 100 ng per serving, an individual would need to consume at least 50 meatballs to ingest a critical dose. These stochastic simulation outputs are summarized in Table 6.

Table 6
Predicted *Staphylococcus aureus* concentrations ($\log_{10}\mathrm{CFUg}^{-1}$), enterotoxin accumulation, and threshold exceedance probabilities under Scenario S1 (ser display counter) and subsequent refrigerated leftover storage (Scenario S3) across10^6Monte Carlo iterations.

Exposure Pathway / Stage	Pathogen Adaptation & Kinetic State	Median ($\log_{10}\mathrm{CFUg}^{-1}$)	95th Percentile ($\log_{10}\mathrm{CFUg}^{-1}$)	Maximum ($\log_{10}\mathrm{CFUg}^{-1}$)	Exceedance Probability $P\left(C \geq 5.0\log_{10}\mathrm{CFUg}^{-1}\right)$	Estimated SE Exposure (ng/meatball)	Min Mea Inta reac 100
Retail Cold Storage (Preopening baseline transition)	$\mu_{\mathrm{cold}} \leq 0.091\mathrm{h}^{-1}$ $P^{\mathrm{no_lag}}_{\mathrm{cold}} = 0.120$	2.27	3.29	3.71	0	0.00 (< CD)	—
Lunch Service (S1) (Midday peak, 0–4 h display)	$\mu_{S1} \leq 0.461\mathrm{h}^{-1}$ $P^{\mathrm{no_lag}}_{\mathrm{S1\text{-}lunch}} = 0.275$	2.29	3.42	3.85	0	0.00 (< CD)	—
Post-Lunch Leftovers (S3 ex-S1) (Cold holding, $t_m = 8\mathrm{h}$)	$\mu_{\mathrm{cold}} \leq 0.091\mathrm{h}^{-1}$ $P^{\mathrm{no_lag}}_{\mathrm{S1\text{-}lunch}} = 0.275$	4.01	5.05	5.90	3.00×10^{-4}(0.03%)	≤ 2.00(< CD)	≥ 5 mea (1.2
Dinner Service (S1) (Extended counter display, 8–12 h)	Continuous daytime holding $P^{\mathrm{no_lag}}_{\mathrm{S1\text{-}dinner}} = 0.321$	2.37	3.51	5.08	8.65×10^{-3}(0.87%)	≤ 1.00(< CD)	≥ 1 mea (2.5
Post-Dinner Leftovers (S3 ex-S1) (Overnight cold holding, $t_m = 12\mathrm{h}$)	$\mu_{\mathrm{cold}} \leq 0.091\mathrm{h}^{-1}$ $P^{\mathrm{no_lag}}_{\mathrm{S1\text{-}dinner}} = 0.321$	4.12	5.12	6.93	1.42×10^{-2}(1.42%)	≤ 2.00(< CD)	≥ 5 mea (1.2

3.3.2. Scenario 2 (S2): Room-temperature service across regions and seasons

Stochastic exposure simulation outputs quantifying *S. aureus* population kinetics, critical enterotoxigenic threshold exceedance probabilities, and concomitant staphylococcal enterotoxin (SE) yields under regional ambient room-temperature display (Scenario S2) and subsequent leftover cold-holding storage (Scenario S3) are summarized in Table 7.

Predicted *Staphylococcus aureus* population kinetics, critical threshold exceedance probabilities [$P\left(C \geq 5.0 \log_{10}\mathrm{CFU\,g^{-1}}\right)$], and staphylococcal e

Season & Geographical Region	T_{room} (°C)	Mean $\mu_{S2}(\mathrm{h^{-1}})$	$P\left(\lambda_{S2} \leq 4.0\mathrm{h}\right)$ (%)	S2 Median ($\log_{10}\mathrm{CFU\,g^{-1}}$)	S2 95th ($\log_{10}\mathrm{CFU\,g^{-1}}$)	S2 Max ($\log_{10}\mathrm{CFU\,g^{-1}}$)	S2 $P(C \geq 5.0)$	S2 SE
Winter (All 7 regions)	0–14	0.000–0.022	0.1–19.4%	2.28–2.29	3.41–3.42	3.72–3.97	0	0.000
Spring (All 7 regions)	4–24	0.044–0.181	22.7–49.5%	2.30–2.38	3.43–3.52	4.16–5.33	$0\text{--}4.36 \times 10^{-5}$	0.000
Autumn (All 7 regions)	4–27	0.075–0.290	28.6–62.0%	2.32–2.45	3.45–3.64	4.80–5.80	$0\text{--}1.10 \times 10^{-3}$	0.000
Summer – Black Sea	16–30	0.384	71.6%	2.51	3.80	7.00	4.16×10^{-3} (0.42%)	0.166
Summer – Eastern Anatolia	13–31	0.352	66.2%	2.49	3.76	7.93	4.54×10^{-3} (0.45%)	0.096
Summer – Marmara	19–33	0.498	81.2%	2.60	4.06	7.93	9.78×10^{-3} (0.98%)	1.378
Summer – Central Anatolia	16–31	0.404	72.8%	2.53	3.84	7.93	5.10×10^{-3} (0.51%)	0.071
Summer – Aegean	19–35	0.532	82.2%	2.62	4.16	7.93	1.37×10^{-2} (1.37%)	1.995
Summer – Mediterranean	22–35	0.592	84.6%	2.67	4.30	7.93	1.66×10^{-2} (1.66%)	1.765
Summer – SE Anatolia	21–38	0.615	85.1%	2.69	4.38	7.93	2.11×10^{-2} (2.11%)	2.760

Notes: Meatballs are standardized at 25 g per meatball. In Scenario S3 (ex-S2), post-lunch ambient leftovers are transferred to closed refrigeration ($T_{\mathrm{cold}} \sim$ 100 ng acute intoxication threshold ($\mathrm{meatballs_{min}} = 1$). In spring S2, maximum concentrations remained below$5.0 \log_{10}\mathrm{CFU\,g^{-1}}(P = 0)$ in five regions $P = 4.36 \times 10^{-5}$). In autumn S2, maximum concentrations remained below$5.0 \log_{10}\mathrm{CFU\,g^{-1}}(P = 0)$ in four regions ($4.80\text{--}4.94 \log_{10}\mathrm{CFU\,g^{-1}}$), but e ;$P = 1.10 \times 10^{-3}$) regions.

3.3.2.1 Spatiotemporal Variation in Growth Kinetics ($\varvec{\mu}_{\varvec{S2}}$ and $\varvec{\lambda}_{\varvec{S2}}$)

Under Scenario S2, pathogen proliferation was governed by seasonal and regional indoor ambient temperatures ($T_{\mathrm{room},i,j}$; Table 1). Specific growth rates ($\mu_{S2,i,j}$) exhibited significant climate-driven divergence across geographical regions and seasons (One-way ANOVA, $p < 0.001$). The highest mean specific growth rates occurred during the summer across all regions (μ range: $0.352\text{--}0.615\mathrm{h^{-1}}$), followed by autumn ($0.075\text{--}0.290\mathrm{h^{-1}}$) and spring ($0.044\text{--}0.181\mathrm{h^{-1}}$), whereas replication was substantially suppressed in the winter ($0.000\text{--}0.022\mathrm{h^{-1}}$).

Geographically, during summer, the highest mean growth rates ($\mu_{S2,i,j}$) were concentrated in Southeastern Anatolia ($0.615\mathrm{h^{-1}}$), followed by the Mediterranean ($0.592\mathrm{h^{-1}}$) and the Aegean and Marmara/Central regions (up to $0.532\mathrm{h^{-1}}$), whereas the lowest mean rates occurred in the cooler Black Sea coast ($0.384\mathrm{h^{-1}}$) and continental Eastern Anatolia ($0.352\mathrm{h^{-1}}$) (Table 7).

The lag time varied inversely with ambient holding temperature. In the retail exposure model, active cell division during the $4.0\mathrm{h}$lunch service window (t_{S2}) occurred only when the operative lag time was resolved within that holding timeframe ($\lambda_{S2,i,j} \leq 4.0\mathrm{h}$). The probability of resolving the lag time within $4.0\mathrm{h}$was highest in summer ($66.2\text{--}85.1\%$), moderate in autumn ($28.6\text{--}62.0\%$) and spring ($22.7\text{--}49.5\%$), and lowest in winter ($0.1\text{--}19.4\%$) (Table 7).

3.3.2.2. Bacterial Proliferation and Enterotoxin Production in Single-Meal Serving

Stochastic exposure modelling demonstrated pronounced climate-driven differences in the *S. aureus* population concentration and staphylococcal enterotoxin (SE) accumulation at consumption (Table 7; Fig. 2).

During winter, median ($2.28\text{--}2.29 \log_{10}\mathrm{CFU\,g^{-1}}$) and 95th percentile ($3.41\text{--}3.42 \log_{10}\mathrm{CFU\,g^{-1}}$) concentrations showed minimal proliferation across all regions, while maximum bacterial concentrations peaked between 3.72 and $3.97 \log_{10}\mathrm{CFU\,g^{-1}}$, remaining strictly below the enterotoxigenic induction threshold ($5.0 \log_{10}\mathrm{CFU\,g^{-1}}$) across all geographical zones ($P\left(C \geq 5.0 \log_{10}\mathrm{CFU\,g^{-1}}\right) = 0$; Table 7). During the transitional spring and autumn

seasons, central tendency loads remained moderate—with medians of $2.30\text{--}2.38 \log_{10}\mathrm{CFU\,g^{-1}}$ in spring and $2.32\text{--}2.45 \log_{10}\mathrm{CFU\,g^{-1}}$ in autumn, and 95th percentiles of $3.43\text{--}3.52$ and $3.45\text{--}3.64 \log_{10}\mathrm{CFU\,g^{-1}}$, respectively. While extreme tail iterations in cooler and temperate zones remained below $5.0 \log_{10}\mathrm{CFU\,g^{-1}}$ ($4.16\text{--}4.93 \log_{10}\mathrm{CFU\,g^{-1}}$ in spring; $4.80\text{--}4.94 \log_{10}\mathrm{CFU\,g^{-1}}$ in autumn), rare upper-tail iterations surpassed the induction threshold in Southeastern Anatolia ($5.19 \log_{10}\mathrm{CFU\,g^{-1}}$; $P = 1.75 \times 10^{-5}$) and the Mediterranean region ($5.33 \log_{10}\mathrm{CFU\,g^{-1}}$; $P = 4.36 \times 10^{-5}$) during spring, as well as in the Aegean ($5.02 \log_{10}\mathrm{CFU\,g^{-1}}$; $P = 4.15 \times 10^{-5}$), Southeastern Anatolia ($5.41 \log_{10}\mathrm{CFU\,g^{-1}}$; $P = 2.11 \times 10^{-4}$), and Mediterranean ($5.80 \log_{10}\mathrm{CFU\,g^{-1}}$; $P = 1.10 \times 10^{-3}$) regions during autumn (Table 7).

Conversely, unchilled summer holding yielded substantially elevated bacterial loads. Regional median concentrations ranged from $2.49 \log_{10}\mathrm{CFU\,g^{-1}}$ in Eastern Anatolia to $2.69 \log_{10}\mathrm{CFU\,g^{-1}}$ in Southeastern Anatolia. The 95th percentiles rose from $3.76 \log_{10}\mathrm{CFU\,g^{-1}}$ in Eastern Anatolia and $3.80 \log_{10}\mathrm{CFU\,g^{-1}}$ along the Black Sea coast to $4.30 \log_{10}\mathrm{CFU\,g^{-1}}$ in the Mediterranean region and $4.38 \log_{10}\mathrm{CFU\,g^{-1}}$ in Southeastern Anatolia, while extreme tail iterations reached the matrix carrying capacity of $7.93 \log_{10}\mathrm{CFU\,g^{-1}}$ across all regions except the Black Sea coast ($7.00 \log_{10}\mathrm{CFU\,g^{-1}}$). Critical threshold exceedance probabilities during summer spanned from 4.16×10^{-3} (0.42%) along the Black Sea coast, 4.54×10^{-3} (0.45%) in Eastern Anatolia, and 5.10×10^{-3} (0.51%) in Central Anatolia to 9.78×10^{-3} (0.98%) in Marmara, 1.37×10^{-2} (1.37%) in the Aegean region, 1.66×10^{-2} (1.66%) in the Mediterranean region, and 2.11×10^{-2} (2.11%) in Southeastern Anatolia. Corresponding maximum predicted enterotoxin concentrations during summer ranged from $0.071 \mathrm{ng\,g^{-1}}$ in Central Anatolia, $0.096 \mathrm{ng\,g^{-1}}$ in Eastern Anatolia, and $0.166 \mathrm{ng\,g^{-1}}$ along the Black Sea coast to $1.378 \mathrm{ng\,g^{-1}}$ in Marmara, $1.765 \mathrm{ng\,g^{-1}}$ in the Mediterranean region, $1.995 \mathrm{ng\,g^{-1}}$ in the Aegean region, and $2.760 \mathrm{ng\,g^{-1}}$ in Southeastern Anatolia. Outside summer, enterotoxin synthesis remained absent ($0.000 \mathrm{ng\,g^{-1}}$) across all regions in winter and spring, whereas trace upper-tail accumulation occurred during autumn in Southeastern Anatolia ($0.014 \mathrm{ng\,g^{-1}}$) and the Mediterranean region ($0.019 \mathrm{ng\,g^{-1}}$) (Table 7).

From a toxicological standpoint, achieving the minimum critical dose ($100 \mathrm{ng}$ of ingested enterotoxin) under Scenario S2 during summer would require the consumption of $\approx 2 \mathrm{standard\text{\:}meatballs\text{\:}(50g)}$ in Southeastern Anatolia ($69.0 \mathrm{ng/meatball}$) and the Aegean region ($49.9 \mathrm{ng/meatball}$), and $\approx 3 \mathrm{\:meatballs\text{\:}(75g)}$ in the Mediterranean ($44.1 \mathrm{ng/meatball}$) and Marmara ($34.5 \mathrm{ng/meatball}$) regions, whereas substantially larger intakes would be needed in the Black Sea ($\approx 24 \mathrm{\:meatballs;\ 600g}$), Eastern Anatolia ($\approx 42 \mathrm{\:meatballs;\ 1.05kg}$), and Central Anatolia ($\approx 57 \mathrm{\:meatballs;\ 1.43kg}$) zones. During autumn, reaching the critical dose in Southeastern Anatolia and the Mediterranean region would require $\geq 206 \mathrm{\:meatballs\text{\:}(\geq 5.15kg)}$ (Table 7).

3.3.2.3. Microbial Proliferation and Enterotoxin Accumulation in Refrigerated Leftovers (Scenario S3)

Scenario S3 evaluated the consumer-phase cold storage of leftovers held at room temperature during service and subsequently refrigerated ($T_{\mathrm{cold}} \sim \mathrm{Uniform}\left(4.0, 8.0\,^{\circ}\mathrm{C}\right)$) for a holding interval of $t_m = 8\mathrm{h}$ (post-lunch). Proliferation of *S. aureus* and subsequent enterotoxin accumulation during this stage were governed by the residual kinetic state and biomass accumulated upstream during Scenario S2 (Table 7).

Stochastic simulations indicated that *S. aureus* concentrations and critical threshold exceedance probabilities ($P\left(C \geq 5.0 \log_{10}\mathrm{CFU\,g^{-1}}\right)$) in refrigerated leftovers were strongly stratified by season and geographical region. During winter, central tendency loads remained low across all zones, with medians of $2.29\text{--}2.30 \log_{10}\mathrm{CFU\,g^{-1}}$ and 95th percentiles of $3.43\text{--}3.44 \log_{10}\mathrm{CFU\,g^{-1}}$, while rare upper-tail iterations reached maximum concentrations of $5.91 \log_{10}\mathrm{CFU\,g^{-1}}$ (Eastern Anatolia) to $6.83 \log_{10}\mathrm{CFU\,g^{-1}}$ (Mediterranean), corresponding to low exceedance probabilities ranging from 1.57×10^{-5} to 4.44×10^{-5} (Table 7). During the transitional spring and autumn seasons, medians remained moderate at $2.31\text{--}2.40 \log_{10}\mathrm{CFU\,g^{-1}}$ and $2.33\text{--}2.47 \log_{10}\mathrm{CFU\,g^{-1}}$, with 95th percentiles of $3.46\text{--}3.56$ and $3.48\text{--}3.68 \log_{10}\mathrm{CFU\,g^{-1}}$, respectively; however, upper-tail maxima surpassed the $5.0 \log_{10}\mathrm{CFU\,g^{-1}}$ induction threshold across all regions, spanning $6.14\text{--}7.93 \log_{10}\mathrm{CFU\,g^{-1}}$ in spring ($P = 1.12 \times 10^{-4}$ in Eastern Anatolia to 7.67×10^{-4} in the Mediterranean region) and $6.49\text{--}7.93 \log_{10}\mathrm{CFU\,g^{-1}}$ in autumn ($P = 1.66 \times 10^{-4}$ in Central Anatolia to 2.74×10^{-3} in the Mediterranean region) (Table 7).

In contrast, refrigerated leftovers originating from unchilled summer holding exhibited substantially higher bacterial distributions across all regions. Regional median concentrations ranged from $2.51 \log_{10}\mathrm{CFU\,g^{-1}}$ in Eastern Anatolia and $2.53 \log_{10}\mathrm{CFU\,g^{-1}}$ along the Black Sea coast to $2.70 \log_{10}\mathrm{CFU\,g^{-1}}$ in the Mediterranean region and $2.71 \log_{10}\mathrm{CFU\,g^{-1}}$ in Southeastern Anatolia. Corresponding 95th percentiles rose from $3.84 \log_{10}\mathrm{CFU\,g^{-1}}$ in Eastern Anatolia and $3.86 \log_{10}\mathrm{CFU\,g^{-1}}$ along the Black Sea coast to $4.26 \log_{10}\mathrm{CFU\,g^{-1}}$ in the Aegean region, $4.39 \log_{10}\mathrm{CFU\,g^{-1}}$ in the Mediterranean region, and $4.48 \log_{10}\mathrm{CFU\,g^{-1}}$ in Southeastern Anatolia, while extreme upper-tail iterations reached the matrix carrying capacity of $7.93 \log_{10}\mathrm{CFU\,g^{-1}}$ across all seven geographical regions (Table 7). Summer threshold exceedance probabilities in refrigerated leftovers ranged from 6.27×10^{-3} (0.63%) along the Black Sea coast, 6.71×10^{-3} (0.67%) in Eastern Anatolia, and 8.09×10^{-3} (0.81%) in Central Anatolia to 1.37×10^{-2} (1.37%) in Marmara, 1.80×10^{-2} (1.80%) in the Aegean region, 2.18×10^{-2} (2.18%) in the Mediterranean region, and 2.64×10^{-2} (2.64%) in Southeastern Anatolia (Table 7).

Peak enterotoxin yields were observed in summer leftovers across all seven geographical regions, reaching the upper-bound maximum of $5.171 \mathrm{ng\,g^{-1}}$ ($129.28 \mathrm{ng\,per\ 25g\,meatball}$) in every region. Assuming a standard commercial meatball mass of $25\mathrm{g}$, ingestion of a single $25\mathrm{g}$ meatball from unrefrigerated summer leftovers is sufficient to exceed the acute intoxication threshold ($100\mathrm{ng}$). In contrast, during non-summer seasons, upper-tail enterotoxin accumulation remained substantially lower—spanning $0.014\text{--}0.024 \mathrm{ng\,g^{-1}}$ ($0.34\text{--}0.60 \mathrm{ng/meatball;\ \geq 168\text{\:}meatballs\text{\:}or}$

$\geq 4.20\mathrm{kg}$to reach $100\mathrm{ng}$) in winter, $0.044\text{--}0.525\mathrm{ngg}^{-1}$ ($1.10\text{--}13.11\mathrm{ng/meatball}$; $\geq 8\,\mathrm{meatballs}$or $\geq 200\mathrm{g}$) in spring, and $0.081\text{--}1.805\mathrm{ngg}^{-1}$ ($2.04\text{--}45.12\mathrm{ng/meatball}$; $\geq 3\,\mathrm{meatballs}$or $\geq 75\mathrm{g}$) in autumn (Table 7).

3.4. Global Sensitivity Analysis of Bacterial Proliferation and Enterotoxin Accumulation

Global sensitivity analysis (Spearman rank correlation, r_s) revealed the primary drivers governing the final *S. aureus* concentration ($C_{\mathrm{stage}}^{\mathrm{comp}}$) and staphylococcal enterotoxin yield (SE_{stage}) in the critical exposure pathways: Scenario S1 extended dinner display and Scenario S2 summer room holding (Table 8).

Table 8

Global sensitivity analysis (Spearman rank correlation coefficients, r_s) of stochastic model parameters and intermediate determinants on terminal *S. aureus* enterotoxin yield (SE_{stage}) in commercial *çiğ köfte*.

Target Model Endpoint	Evaluated Parameter / Determinant	Symbol	Spearman Rank Correlation (r_s)	Statistical Significance (p value)	Et D S In R
FinalConcentration($C_{\text{stage}}^{\text{comp}}$, $\log_{10}\text{CFUg}^{-1}$)	Ambient / Display Temperature	T_{S1} / T_{room}	$+0.72\text{to}+0.89$	$p < 0.001$	P (D st dı 1)
	Display / Holding Duration	$t_{\text{service}}(t_{S1\text{-dinner}}, t_{S2})$	$+0.68\text{to}+0.81$	$p < 0.001$	P (D st dı 2)
	Reference Specific Growth Rate	$\mu_{\max,22\,^\circ\text{C}}$	$+0.31\text{to}+0.44$	$p < 0.01$	P (M st dı 3)
	Reference Adaptation Lag Time	$\lambda_{22\,^\circ\text{C}}$	$-0.24\text{to}-0.38$	$p < 0.05$	N (M st dı 4)
	Initial Matrix Contamination	$S.\,\text{aureus}_0$	$\lvert r_s\rvert < 0.10$	$p > 0.05$ (NS)	N in
EnterotoxinYield(SE_{stage}, ngg^{-1}; $D_{\text{SE,\:meatball}}$, ng/meatball)	Terminal Pathogen Concentration*	$C_{\text{stage}}^{\text{comp}}$	$+0.84\text{to}+0.93$	$p < 0.001$	P (P in dı R
	Ambient Display Temperature	T_{room}	$+0.58\text{to}+0.74$	$p < 0.001$	P (K up st dı 2)
	Elapsed Exposure Window	$t_{\text{service}}(t_{S1\text{-dinner}}, t_{S2})$	$+0.52\text{to}+0.69$	$p < 0.001$	P (K up st dı 3)
	Reference Adaptation Lag Time	$\lambda_{22\,^\circ\text{C}}$	$-0.36\text{to}-0.51$	$p < 0.01$	N (M st dı 4)
	Enterotoxigenic Strain Fraction	P_{ET}	$+0.28\text{to}+0.39$	$p < 0.01$	P (S pı 5)
	Baseline Microbial Load	$S.\,\text{aureus}_0$	$\lvert r_s\rvert < 0.10$	$p > 0.05$ (NS)	N in

The bacterial concentration at consumption was predominantly driven by the holding temperature (T_{S1} or T_{room}; $r_s = +0.72\text{to}+0.89$, $p < 0.001$) and elapsed display duration ($t_{S1\text{-dinner}}$ or t_{S2}; $r_s = +0.68\text{to}+0.81$, $p < 0.001$), followed by moderate contributions from the reference specific growth rate ($\mu_{\max,22\,^\circ\text{C}}$; $r_s = +0.31\text{to}+0.44$, $p < 0.01$) and adaptation lag time ($\lambda_{22\,^\circ\text{C}}$; $r_s = -0.24\text{to}-0.38$, $p < 0.05$).

Staphylococcal enterotoxin accumulation was governed primarily by the intermediate terminal *S. aureus* population concentration ($C_{\text{stage}}^{\text{comp}}$, $r_s = +0.84\text{to}+0.93$, $p < 0.001$), followed by the upstream stochastic drivers: ambient display temperature (T_{room}; $r_s = +0.58\text{to}+0.74$,

$p < 0.001$), elapsed exposure duration ($t_{\text{service}};\ r_s = +0.52\text{to} + 0.69,\ p < 0.001$), an inverse correlation with the reference adaptation lag time at 22°C ($\lambda_{22\,^\circ\text{C}};\ r_s = -0.36\text{to} - 0.51,\ p < 0.01$), and the enterotoxigenic strain fraction ($P_{\text{ET}};\ r_s = +0.28\text{to} + 0.39,\ p < 0.01$). Initial matrix contamination ($S.\,\text{aureus}_0$) had a negligible influence on both terminal concentration and enterotoxin formation ($|r_s| < 0.10,\ p > 0.05$).

These sensitivity rankings confirm that ambient display temperature and cumulative unrefrigerated holding duration represent the decisive critical control points (CCPs) for preventing staphylococcal enterotoxin synthesis and eliminating exposure in commercial *çiğ köfte* supply chains.

4. DISCUSSION

4.1. Exposure Dynamics, Matrix Effects, and Public Health Implications

Although traditionally prepared with raw minced meat ("Tartar à la Turca"), the commercial formulation of *çiğ köfte* was legally reformed following a widespread trichinellosis outbreak in İzmir in 2004 (Akkoc et al., 2009). The Turkish Food Codex strictly banned raw meat in commercial ready-to-eat (RTE) products via Communiqué No. 2012/74 (Turkish Food Codex, 2012), a measure reaffirmed by Communiqué No. 2018/52 (Turkish Food Codex, 2019) and standardized as “Tartar A la Turca (Meatless)” under TS 13804 (TSE, 2018). Since 2012, commercial *çiğ köfte* has consisted exclusively of a meatless matrix composed of bulgur, vegetable pastes, oils, and spices. Accordingly, only peer-reviewed retail surveys conducted after 2012 were incorporated to model the initial staphylococcal contamination in this exposure assessment.

Baseline retail contamination was parameterized using data from Delikanlı et al. (2014), the most comprehensive post-2012 survey quantifying coagulase-positive staphylococci across commercial plant-based *çiğ köfte*. Crucially, the maximum reported initial concentration of $3.71\log_{10}\text{CFU}\cdot\text{g}^{-1}$ remains well below the critical threshold of $5.0\log_{10}\text{CFU}\cdot\text{g}^{-1}$, universally recognized as the minimum population concentration required to trigger detectable staphylococcal enterotoxin (SE) synthesis (Lindqvist et al., 2002; Sirotamarat et al., 2022). Consequently, intact *çiğ köfte* exiting production facilities or entering retail displays poses a negligible immediate toxigenic hazard. The accumulation of preformed enterotoxins is therefore entirely contingent upon downstream thermal abuse, extended display counter holding, or inappropriate storage that allows bacterial amplification beyond this induction threshold.

4.2. Kinetic Heterogeneity and Food Matrix Interactions

Primary kinetic modelling revealed no statistically significant differences in lag time ($\lambda_{22\,^\circ C};\ p = 0.661$) or growth rate ($\mu_{\text{max}22\,^\circ\text{C}};\ p = 0.393$) among the three *S. aureus* strains at 22°C. However, pronounced replicate-to-replicate variability occurred, aligning with findings by Medveďová et al. (2019) regarding initial physiological states, microenvironmental heterogeneity, and density-dependent lag phenomena. The dispersion in growth rates ($\mu_{\text{max},\,22\,^\circ\text{C}}$) across replicates reflects strain-level diversity and matrix interactions (Alreshidi et al., 2022; Silva et al., 2023). Specific metabolic adaptations, particularly amino acid utilization and osmoregulation, modulate replication capacity in dense food matrices (Alreshidi et al., 2022) irrespective of the pH and a_w values (Kang et al., 2010). Unlike homogeneous liquid media, the solid microarchitecture of *çiğ köfte* generates localized moisture and substrate gradients that alter lag times (Lindqvist, 2006; Tango et al., 2016; Valík et al., 2008).

Notably, empirical kinetics in *çiğ köfte* were significantly more permissive than broth-based ComBase predictions were. While the ComBase growth rate (0.1019h^{-1}) matched the lower range of experimental values, its predicted lag times ($18.31\text{hat }22\,^\circ\text{C};\ 8.07\text{hat }37\,^\circ\text{C}$) vastly exceeded the empirical observations ($0.00\text{to}11.66\text{h}$). Liquid-broth models fail to integrate the protective microniches and concentrated nutrient accessibility characteristics of bulgur–spice paste, resulting in an underestimation of real-world proliferation. These findings confirm that matrix-specific challenge testing is essential for avoiding dangerous underestimations in quantitative exposure assessments. In *çiğ köfte* following the challenge test, the estimated maximum population concentration $[S.\ aureus]_{\max}$ was parameterized at the upper standard error bound of 7.93 $\log_{10}$ CFU g^{-1} (7.31 + 0.62 $\log_{10}$ CFU g^{-1}) on the basis of the highest empirical stationary-phase concentration observed in strain D4508 (Rep 3), representing a conservative, health-protective worst-case scenario (Table 5). While extrapolating growth kinetics across $0\text{--}38\,^\circ\text{C}$from single-temperature challenge data ($22\,^\circ\text{C}$) via literature-derived cardinal temperatures assumes multiplicative gamma independence without matrix-induced shifts in $T_{\min}$ or $T_{\max}$, anchoring μ_{opt} in empirical *çiğ köfte* challenge tests provides substantially greater realism than broth-based predictions.

Although the *çiğ köfte* matrix was sterilized by autoclaving (121°C for 15 min) to eliminate indigenous background microbiota and ensure unambiguous kinetic enumeration of the target pathogen, this experimental setup was intentionally designed as a conservative, health-protective “worst-case scenario”. The physicochemical properties (a_w and pH) were measured before and after sterilization and did not significantly change ($p > 0.05$). In unsterilized, traditional plant-based foods, endogenous background microflora, particularly lactic acid bacteria (LAB) originating from vegetable pastes and fermented spices, typically exhibit competitive microbial antagonism, constraining pathogen growth through nutrient competition, spatial exclusion, and the accumulation of inhibitory metabolites. By suppressing competitive microflora, *S. aureus* was allowed to replicate unhindered at its matrix-specific maximum kinetic boundary. In quantitative microbial exposure assessment (QMEA), modelling unconstrained growth without competitive inhibition represents a standard fail-safe methodology: it anticipates modern commercial manufacturing where strict sanitation protocols reduce background bacterial loads and accounts for postprocessing manual recontamination where *S. aureus* is introduced onto clean contact surfaces or into microniches devoid of active competitors. Consequently, kinetic parameters determined in the autoclaved matrix prevent any dangerous underestimation of pathogen proliferation and enterotoxin expression, ensuring appropriately robust and precautionary public health risk estimates.

Nevertheless, thermal sterilization at 121°C may also attenuate heat-labile antimicrobial phytochemicals present in raw garlic, lemon juice, and spices while increasing starch gelatinization in bulgur, further reinforcing the conservative, worst-case nature of the derived kinetic parameters.

4.3. Temperature Abuse Dynamics across Regions and Seasons

Challenge testing at $22\ ^{\circ}$ Crevealed that *S. aureus* can initiate growth without delay, with two biological replicates exhibiting zero lag time ($\lambda_{22^{\circ}\mathrm{C}} = 0.00\mathrm{h}$; Table 5). Moreover, simulated preopening refrigeration ($T_{\mathrm{cold}} = 4\text{--}8^{\circ}\mathrm{C};\ t_{\mathrm{cold}} = 96\mathrm{h}$) exhausted the lag phase in 12% of the packages ($P_{\mathrm{cold}}^{\mathrm{no_lag}} = 0.12$), allowing a significant fraction of the retail batches to undergo immediate exponential division upon display opening.

As the temperature approached the optimum for *S. aureus* (37°C), replication accelerated exponentially. At 37°C, the estimated lag duration decreased to a median of 1.01 h (range: 0–6.88 h), which was concurrent with a surge in specific growth rates. These kinetic shifts align with the findings of Anandita et al. (2024) and Juneja et al. (2025) on thermal abuse in RTE foods. Unrefrigerated temperatures above 25°C critically increase pathogen multiplication (Ahmed et al., 2023; Valero et al., 2009), creating high-risk niches reminiscent of those observed in sliced meats (Ahmed et al., 2023), kimbap (Bahk et al., 2006), and cooked rice dishes (Lu et al., 2020).

Conversely, counter conditions (4–15°C) imposed robust bacteriostatic control primarily by extending lag times. Temperatures below 15°C severely constrain metabolic recovery; lag times exceed 98 h at 8°C in milk ($\mu \approx 0.005\mathrm{h}^{-1}$; Medveďová et al., 2010), with negligible growth occurring below 8°C (Xie et al., 2020). Complete growth arrest in lower-temperature counter iterations (where $T_{S1} \le T_{min}$ or λ_{S1} exceeded the service window, occurring in 67.9–72.5% of iterations) reflects metabolic dormancy (Medveďová et al., 2019; Onyango et al., 2012). Even after lag resolution, viable populations remained strictly below the $5.0\log_{10}\mathrm{CFU}\cdot\ \mathrm{g}^{-1}$ toxigenic threshold across all realistic counter display durations.

Two structural modelling assumptions warrant consideration when interpreting these seasonal outputs. First, indoor ambient temperatures in Scenario S2 were parameterized using regional outdoor meteorological medians (AccuWeather, 2025). While this accurately reflects thermal heat loads in non-air-conditioned retail shops during warm seasons, indoor heating in commercial establishments during winter (typically maintained at 18–22°C) may result in higher actual room temperatures than outdoor winter medians (0–14°C), meaning winter risk estimates represent best-case ambient conditions. Second, two biological replicates exhibited zero lag time at 22°C ($\lambda_{22^{\circ}\mathrm{C}} = 0.00\mathrm{h}$; Table 5); under the work-to-be-done scaling formulation (Eq. 6), these replicates yielded $\lambda_T = 0.00$ hacross all temperatures above T_{min}, contributing conservatively to upper-tail proliferation during cold storage.

4.4. Public Health Exposure: Fresh Meatballs vs. Leftovers

Room-temperature service modelling (Scenario S2) demonstrated marked spatiotemporal risk divergence driven by regional temperature. In winter across all zones, median ($2.28\text{--}2.29\ \log_{10}\mathrm{CFUg}^{-1}$) and 95th-percentile ($3.41\text{--}3.42\ \log_{10}\mathrm{CFUg}^{-1}$) concentrations showed minimal growth, and maximum *S. aureus* populations remained below $3.97\ \log_{10}\mathrm{CFUg}^{-1}$, precluding enterotoxin production. In contrast, summer temperatures in the Central, Aegean, Mediterranean, and Southeastern Anatolian regions elevated 95th-percentile concentrations to $3.84\text{--}4.38\ \log_{10}\mathrm{CFUg}^{-1}$ and drove upper-tail iterations to the matrix carrying capacity of $7.93\ \log_{10}\mathrm{CFUg}^{-1}$—well above the $5.0\ \log_{10}\mathrm{CFUg}^{-1}$ critical induction threshold (Table 7)—yielding predicted SE levels of up to $2.760\mathrm{ngg}^{-1}$. Given the extensive manual shaping involved and the lack of terminal cooking, unchilled summer displays represent the primary exposure vulnerability.

A critical divergence exists between fresh servings and leftovers. During a 4 h ambient service window, enterotoxin accumulation remains moderate ($0.000\text{--}2.760\mathrm{ng}\cdot\ \mathrm{g}^{-1}$ across seasons; $0.071\text{--}2.760\mathrm{ng}\cdot\ \mathrm{g}^{-1}$ in summer). Delivering the 100 ng critical dose requires the consumption of $\approx\ 2\text{:meatballs\:}$(50 g) in Southeastern Anatolia (69.00 ng/meatball) and the Aegean region (49.88 ng/meatball), $\approx\ 3\text{:meatballs\:}$(75 g) in the Mediterranean (44.13 ng/meatball) and Marmara (34.45 ng/meatball) regions, and $\ge\ 24\text{:meatballs}(\ \ge\ 600\mathrm{g})$ **elsewhere**. Although fresh unchilled meatballs seldom trigger acute poisoning, counts near $5.0\ \log_{10}\mathrm{CFU}\cdot\ \mathrm{g}^{-1}$ reflect a microbiological hazard on the verge of active toxigenesis.

The most severe hazard occurs when temperature-abused meatballs are held as leftovers in closed refrigeration (4–8°C) for 8 h (Scenario S3 ex-S2), whereas refrigerated leftovers originating from display counters (Scenario S3 ex-S1, held up to 12 h) remain sub-toxic ($\le\ 2.0\mathrm{ng/meatball}$). The high enterotoxin yields observed in ambient-abused refrigerated leftovers (up to $5.17\mathrm{ng}\cdot\ \mathrm{g}^{-1}$) reflect the cumulative staphylococcal biomass and active toxicity achieved during the preceding daytime ambient display, which remain stable upon refrigeration. Ingestion of just one 25 g meatball delivers up to 129.3 ng of SE, immediately exceeding the 100 ng intoxication threshold for vulnerable consumers. Therefore, the refrigeration retention of room-temperature leftovers constitutes the single highest-risk handling practice in the *çiğ köfte* consumption chain.

In the stochastic modelling framework, enterotoxin accumulation (Eq. 11) was evaluated on the enterotoxigenic subpopulation concentration ($C_{\mathrm{stage}}^{\mathrm{comp_ent}}$, Eq. 10) derived from the terminal bacterial concentration ($C_{\mathrm{stage}}^{\mathrm{comp}}$) at the end of each stage, including secondary leftover refrigeration (Scenario S3). Because the literature-derived minimum growth temperature distribution ($T_{\mathrm{min}} \in\ \left[6.5,10.0\ ^{\circ}\mathrm{C}\right]$) partially overlapped with the refrigeration temperature range ($T_{\mathrm{cold}} \sim\ \mathrm{Uniform}\left(4.0,8.0\ ^{\circ}\mathrm{C}\right)$), upper-tail iterations combining low T_{min} values with exhausted lag phases permitted slow residual proliferation ($\mu_{\mathrm{cold}} \le\ 0.091\mathrm{h}^{-1}$) during the 8–12 h cold-holding window. Although *de novo* staphylococcal enterotoxin synthesis is physiologically inhibited below 10°C under strictly controlled refrigeration (Schmitt et al., 1990; ICMSF, 1996), domestic refrigerators frequently experience thermal fluctuations into the 8–12°C range where both growth and residual toxigenesis can persist. Consequently, evaluating Eq. 11 at the terminal S3 concentration functions as a deliberate, health-protective worst-case proxy for domestic cold-chain abuse, whereas strict adherence to $\le\ 8\ ^{\circ}\mathrm{C}$would stabilize enterotoxin levels at their pre-refrigeration S2 concentrations ($\le\ 69.00\mathrm{ng/meatball}$). Furthermore, although Eq. 11 applies a deterministic log-linear relationship between enterotoxigenic cell density and toxin yield without incorporating inter-strain secretory variance, anchoring the upper-bound kinetic capacity in the enterotoxigenic *sea*-positive reference strain D4508 ensures precautionary, health-protective exposure estimates.

4.5. Methodological Handling of Experimental Outliers in the QMEA

Within parameterized stochastic kinetic distributions, empirical replicates exhibiting minimal lag durations ($\lambda \approx 0.00\text{--}0.29\mathrm{h}$) or elevated replication rates were deliberately retained rather than discarded as anomalous statistical outliers. In predictive microbiology and quantitative microbial exposure assessment (QMEA), the arbitrary exclusion of extreme observations in the absence of documented technical failure, analytical contamination, or procedural artifacts introduces severe structural bias and artificially constrains model variance.

Because solid and semisolid food matrices exhibit inherent spatial, nutritional, and physicochemical microheterogeneity, biological replicate dispersion captures genuine aleatory stochasticity in terms of phenotypic switching, physiological adaptation times, and microniche nutrient accessibility. In QMEA frameworks, consumer safety and food control decisions must be firmly anchored in upper-tail exposure distributions (e.g., 95th and 99th percentiles) rather than central tendency metrics (medians or means). The incorporation of empirical extremes into secondary modelling input distributions ensures that Monte Carlo simulations encompass worst-case physiological adaptation and temperature abuse conditions, ultimately delivering robust, transparent, and public health-protective exposure assessments.

5. CONCLUSION

This study established the first climate-informed predictive exposure model to simulate *Staphylococcus aureus* proliferation and staphylococcal enterotoxin (SE) production in commercial plant-based *çiğ köfte* across 81 provinces and seven geographical regions of Türkiye. By coupling laboratory challenge-test kinetics with regional meteorological profiles and realistic consumer handling pathways, the model successfully captured the biological heterogeneity and exposure dynamics of this traditional ready-to-eat (RTE) food.

These findings demonstrate that holding *çiğ köfte* under active display counter refrigeration (4–15°C) provides effective bacteriostatic control, maintaining bacterial densities strictly below the toxigenic threshold ($5.0\ \log_{10}\mathrm{CFU}\cdot\ \mathrm{g}^{-1}$) with negligible exceedance probability ($P \leq\ 0.0087$, i.e., 0.87%) and sub-toxic enterotoxin levels ($\leq\ 1.0\mathrm{ng/meatball}$). In contrast, warm-season ambient room temperatures (13–38°C) rapidly exhausted the lag phase, driving bacterial growth toward the matrix carrying capacity of $7.93\ \log_{10}\mathrm{CFUg}^{-1}$ and triggering active enterotoxigenesis, with exceedance probabilities reaching 2.11% in Southeastern Anatolia, 1.66% in the Mediterranean region, 1.37% in the Aegean region, and 0.98% in Marmara during summer. Crucially, the exposure assessment revealed that secondary domestic leftovers originating from ambient room display (Scenario S3 ex-S2) represent a critical public health bottleneck, yielding enterotoxin concentrations of up to $5.17\mathrm{ngg}^{-1}$ ($129.3\mathrm{ng}$per 25 g meatball) after 8 h of refrigerated holding. Under this handling pathway, the ingestion of a single 25 g meatball is sufficient to exceed the acute intoxication critical dose (100 ng) for sensitive populations.

A global sensitivity analysis confirmed that the holding temperature ($r_s =\ +\ 0.72\mathrm{to}+0.89$) and display duration ($r_s =\ +\ 0.68\mathrm{to}+0.81$) are the decisive risk drivers. To safeguard consumer health, actionable risk management based on our simulation outputs should prioritize (i) restricting unrefrigerated retail displays to ≤2 h during warm seasons (T ≥ 25°C); (ii) downsizing commercial wholesale packaging from 10 kg to ≤5 kg to accelerate batch turnover; and (iii) immediately discarding unrefrigerated leftovers rather than returning them to domestic refrigeration. Although post-opening manual cross-contamination during portioning was outside the quantitative scope of the present model, these thermal and inventory controls should be complemented by strict glove-changing and hand hygiene protocols during service.

Declarations

Declaration of interest

The authors declare that they have no conflicts of interest.

Funding declaration

This research received no external funding.

Declaration of generative AI and AI-assisted technologies in the writing process

During the preparation of this work, the authors used ChatGPT to edit the grammar of the paper. After using this tool/service, the authors reviewed and edited the content as needed and take full responsibility for the content of the publication.

References

1. 1. Ahmed, S. M., Kassem, G. M. A., Pérez-Rodríguez, F., & Abdel-Naeem, H. H. S. (2023). Application of predictive microbiology in monitoring *S. aureus* growth in raw chicken meat. *Advanced Animal Veterinary Sciences*, 11, 738–746.
2. 2. Akkoc, N., Kuruuzum, Z., Akar, S., Yuce, A., Onen, F., Yapar, N., Ozgenc, O., Turk, M., Ozdemir, D., Avci, M., Guruz, Y., Oral, A. M., Pozio, E., & Izmir Trichinellosis Outbreak Study Group. (2009). A large-scale outbreak of trichinellosis caused by *Trichinella britovi* in Turkey. *Zoonoses and Public Health*, 56(2), 65–70. https://doi.org/10.1111/j.1863-2378.2008.01158.x
3. 3. Alreshidi, M., Dunstan, H., Roberts, T., Bardakci, F., Badraoui, R., Adnan, M., Saeed, M., Alreshidi, F., Albulaihed, Y., & Snoussi, M. (2022). Changes in amino acid metabolism of *S. aureus* following growth to the stationary phase under adjusted growth conditions. *Microorganisms*, *10*(8), 1503.
4. 4. Anandita, A. F., Arief, I. I., & Taufik, E. (2024). Predictive modelling of *S. aureus* growth on beef rendang. *Malaysian Journal of Microbiology*, *20*(4).
5. 5. Angelotti, R., Foter, M. J., & Lewis, K. H. (1961). Time—temperature effects on salmonellae and staphylococci in foods. I. Behavior in refrigerated foods. II. Behavior at warm holding temperatures. *American Journal of Public Health and the Nation's Health*, *51*, 76–88. DOI: 10.2105/ajph.51.1.76.

6. 6. ANSES (The French Agency for Food, Environmental and Occupational Health & Safety). (2011). *S. aureus* and staphylococcal enterotoxins. Data sheet on foodborne biological hazards.
7. 7. Argudín, M. Á., Mendoza, M. C., & Rodicio, M. R. (2010). Food poisoning and *S. aureus* enterotoxins. *Toxins*, 2(7), 1751–1773.
8. 8. Baeza, R., Rossler, C., Mielnicki, D., Zamora, M.C., & Chirife, J. (2009). Theoretical modelling of *Staphylococcus aureus* growth in a cooked meat product kept at ambient temperature using temperature profiles of selected Mexican cities. *Ciencia e Tecnologia de Alimentos, 29*, 81–84. https://doi.org/10.1590/S0101-20612009000100013.
9. 9. Bahk, G. J., Hong, C. H., Oh, D. H., Ha, S. D., Park, K. H., & Todd, E. C. (2006). Modelling the level of contamination of *S. aureus* in ready-to-eat kimbab in Korea. *Journal of Food Protection*, 69(6), 1340–1346.
10. 10. Cagri-Mehmetoglu, A. (2018). Food safety challenges associated with traditional foods of Turkey. *Food Science and Technology*, 38, 1–12.
11. 11. Campagnollo, F. B., Gonzales-Barron, U., Cadavez, V. A. P., Sant'Ana, A. S., & Schaffner, D. W. (2018). Quantitative risk assessment of *Listeria monocytogenes* in traditional Minas cheeses: The cases of artisanal semihard and fresh soft cheeses. *Food control*, *92*, 370–379.
12. 12. Cheung, G. Y., Bae, J. S., & Otto, M. (2021). Pathogenicity and virulence of *S. aureus*. *Virulence*, 12(1), 547–569.
13. 13. Chieffi, D., Fanelli, F., & Fusco, V. (2023). Antimicrobial and biocide resistance in *S. aureus*: genomic features, decontamination strategies, and the role of *S. aureus* complex-related species, with a focus on ready-to-eat food and food-contact surfaces. *Frontiers in Food Science and Technology*, 3, 1165871.
14. 14. Choi, W. S., Son, N., Cho, J. I., Joo, I. S., Han, J. A., Kwak, H. S., Hong, J. H., & Suh, S. H. (2019). Predictive model of *Staphylococcus aureus* growth on egg products *Food Science and Biotechnology, 28*, 913–922. https://doi.org/10.1007/s10068-018-0529-4.
15. 15. De Matos, G. (2013). Contribution à la maîtrise du risque lié à *Staphylococcus aureus* en filière fermière de fromage de chèvre au lait cru en Corse (Doctoral dissertation).
16. 16. Delikanlı, B., Sönmez, B., & Özdemir, Y. (2014). Microbiological Quality of the Meat-Free *Çiğ köfte* Consumed in Bursa City Center. *Harran University Journal of the Faculty of Veterinary Medicine*, 3(1), 13–17.
17. 17. FDA, (2012) Bad bug book: Foodborne pathogenic microorganisms and natural toxins handbook, 2nd ed, US Food and Drug Administration, Silver Spring, p. 87–92.
18. 18. Fisher, E. L., Otto, M., & Cheung, G. Y. (2018). Basis of virulence in enterotoxin-mediated staphylococcal food poisoning. *Frontiers in microbiology*, 9, 436.
19. 19. Gencay, Y. E., Ayaz, N. D., Copuroglu, G., & Erol, I. (2016). Biocontrol of Shiga toxigenic *Escherichia coli* O157:H7 in Turkish raw meatball by bacteriophage. *Journal of Food Safety*, 36(1), 120–131.
20. 20. Güran, H. S., & İlhak, O. İ. (2015). The effects of different storage temperatures and time on the survival of cpe (+) *Clostridium perfringens* type A in *çiğ köfte* (a traditional turkish raw meat product). *Annals of Animal Science*, *15*(1), 237.
21. 21. Hennekinne, J. A., De Buyser, M. L., & Dragacci, S. (2012). *S. aureus* and its food poisoning toxins: characterization and outbreak investigation. *FEMS microbiology reviews*, 36(4), 815–836.
22. 22. ICMSF (1996). *Staphylococcus aureus*. Ch 17 In: Microorganisms in food 5: Microbiological specifications of food pathogens. Blackie Academic and Professional, London, p. 299–333
23. 23. Ingham, S. C., Engel, R. A., Fanslau, M. A., Schoeller, E. L., Searls, G., Buege, D. R., & Zhu, J. (2005). Fate of *S. aureus* on vacuum-packaged ready-to-eat meat products stored at 21 C. *Journal of food protection*, *68*(9), 1911–1915.
24. 24. Juneja, V. K., Osoria, M., Kapoor, H. K., Gupta, P., Salazar, J. K., Shrestha, S., Bag, S. K. & Mishra, A. (2025). A predictive growth model of *S. aureus* during temperature abuse conditions. *Food Research International*, 206, 116032.
25. 25. Kadariya, J., Smith, T. C., & Thapaliya, D. (2014). *Staphylococcus aureus* and staphylococcal food-borne disease: an ongoing challenge in public health. *BioMed Research International, 2014*, 1–9. https://doi.org/10.1155/2014/827965.
26. 26. Kang, H. S., Ha, S. D., Jeong S. W., Jang, M., & Kim, J. C. (2013). Predictive modelling of *Staphylococcus aureus* growth on Gwamegi (semidry Pacific saury) as a function of temperature. *Journal of the Korean Society for Applied Biological Chemistry, 56*, 731–738. https://doi.org/10.1007/s13765-013-3122-9.
27. 27. Kang, K. A., Yoon, K. S., & Kim, Y. W. (2010). Development of predictive growth models for *S. aureus* and *Bacillus cereus* on various food matrices consisting of ready-to-eat (RTE) foods. *Korean Journal for Food Science of Animal Resources*, 30(5), 730–738.
28. 28. Kim, H. J., Griffiths, M. W., Fazil, A. M., & Lammerding, A. M. (2009). Probabilistic risk model for staphylococcal intoxication from pork-based food dishes prepared in food service establishments in Korea. *Journal of Food Protection*, *72*(9), 1897–1908.
29. 29. Knipper, A. D., Crease, T., Guenther, T., Filter, M., & Nauta, M. (2023). Quantitative microbiological risk assessment model for *Campylobacter* in raw milk of dairy cows in Germany. *Microbial Risk Analysis*, *25*, 100274.
30. 30. Koutsoumanis, K. (2001). Predictive modelling of the shelf life of fish under nonisothermal conditions. *Applied and environmental microbiology*, 67(4), 1821–1829.
31. 31. Le Loir, Y., Baron, F., Gautier, M. (2003). *Staphylococcus aureus* and food poisoning *Genetics and Molecular Research*, 2, 63–76. PMID: 12917803.
32. 32. Lindqvist, R. (2006). Estimation of *S. aureus* growth parameters from turbidity data: characterization of strain variation and comparison of methods. *Applied and Environmental Microbiology*, 72(7), 4862–4870.
33. 33. Lindqvist, R., & Lindblad, M. (2008). Quantitative risk assessment of thermophilic *Campylobacter* spp. and cross-contamination during handling of raw broiler chickens evaluating strategies at the producer level to reduce human campylobacteriosis in Sweden. *International Journal of Food Microbiology*, *121*(1), 41–52.

34. 34. Lindqvist, R., Sylvén, S., & Vågsholm, I. (2002). Quantitative microbial risk assessment exemplified by *S. aureus* in unripened cheese made from raw milk. *International Journal of Food Microbiology*, 78(1–2), 155–170.
35. 35. Lu, K. H., Sheen, Y. J., Huang, T. P., Kao, S. H., Cheng, C. L., Hwang, C. A., Sheen, S., Huang, L., & Sheen, L. Y. (2020). Effect of temperature on the growth of *S. aureus* in ready-to-eat cooked rice with pork floss. *Food Microbiology*, 89, 103374.
36. 36. Martin, S. E., & Iandolo, J. J. (2000). Staphylococcus. In *Encyclopedia of Food Microbiology*, Vol **3** (R.K. Robinson, C.A. Batt and P.D. Patel, eds.) pp. 2062–2065, Academic Press, New York.
37. 37. Medveďová, A., & Valík, Ľ. (2012). *Staphylococcus aureus*: characterization and quantitative growth description in milk and artisanal raw milk cheese production. Eissa AA. ed. Structure and Function of Food Engineering. In Tech, Rijeka, Croatia: pp. 71–102.
38. 38. Medveďová, A., Havlíková, A., Lehotová, V., & Valík, Ľ. (2019). *S. aureus* 2064 growth as affected by temperature and reduced water activity. *Italian Journal of Food Safety*, 8(4), 8287.
39. 39. Medveďová, A., Valík, Ľ., & Studeničová, A. (2010). The effect of temperature and water activity on the growth of *S. aureus*. *Czech Journal of Food Sciences*, 27(Special Issue 2), S-II.
40. 40. Missiakas, D. M., & Schneewind, O. (2013). Growth and laboratory maintenance of *Staphylococcus aureus. Current Protocols in Microbiology*, CHAPTER 9: Unit–9C.1. DOI: 10.1002/9780471729259.mc09c01 s28.
41. 41. Nauta, M. J., Litman, S., Barker, G. C., & Carlin, F. (2003). A retail and consumer phase model for exposure assessment of *Bacillus cereus*. *International Journal of Food Microbiology*, 83(2), 205–218.
42. 42. Onyango, L. A., Dunstan, R. H., Gottfries, J., von Eiff, C., & Roberts, T. K. (2012). Effect of low temperature on growth and ultrastructure of *S.* spp. *PloS one*, 7(1), e29031.
43. 43. Rosso, L., Lobry, J. R., & Flandrois, J. P. (1993). An unexpected correlation between cardinal temperatures of microbial growth highlighted by a new model. *Journal of Theoretical Biology*, 162(4), 447–463. https://doi.org/10.1006/jtbi.1993.1099
44. 44. Russell, N. J., & Gould, G. W. (2003). *Food Preservatives* (2nd ed.). Kluwer Academic/Plenum Publishers, New York.
45. 45. Schmitt, M., Schuler-Schmid, U., & Schmidt-Lorenz, W. (1990). Temperature limits of growth, TNase and enterotoxin production of *Staphylococcus aureus* strains isolated from foods. *International Journal of Food Microbiology, 11*, 1–19. https://doi.org/10.1016/0168-1605(90)90036-5.
46. 46. Silva, B. N., Coelho-Fernandes, S., Teixeira, J. A., Cadavez, V., & Gonzales-Barron, U. (2023). Dynamic Modelling to Describe the Effect of Plant Extracts and Customized Starter Culture on *S. aureus* Survival in Goat's Raw Milk Soft Cheese. *Foods*, 12(14), 2683.
47. 47. Sirotamarat, P., Hinjoy, S., Chuxnum, T., Wongkumma, A., Somboonna, N., & Nuanualsuwan, S. (2022). Quantitative risk assessment of Staphylococcal Enterotoxin A (SEA) in pork in metropolitan Bangkok, Thailand. *LWT*, 168, 113942.
48. 48. Tango, C. N., Park, J. H., & Oh, D. H. (2016). An experimental validated in silico model to assess *S. aureus* growth kinetics on different pork products. *Journal of Applied Microbiology*, *120*(3), 684–696.
49. 49. Tirloni, E., Stella, S., De Knegt, L. V., Gandolfi, G., Bernardi, C., & Nauta, M. J. (2018). A quantitative microbial risk assessment model for *Listeria monocytogenes* in RTE sandwiches. *Microbial Risk Analysis*, *9*, 11–21.
50. 50. Tsaloumi, S., Aspridou, Z., Tsigarida, E., Gaitis, F., Garofalakis, G., Barberis, K., & Koutsoumanis, K. (2021). Quantitative risk assessment of *Listeria monocytogenes* in ready-to-eat (RTE) cooked meat products sliced at retail stores in Greece. *Food Microbiology*, *99*, 103800.
51. 51. TSE (Turkish Standards Institute). (2018). *Tartar A la Turca (meatless)* (TS 13804). Turkish Standards Institute. Published on 15 January 2018.
52. 52. Turkish Food Codex. (2012). *Meat and meat products communiqué* (No. 2012/74). Official Gazette, 28488, 5 December 2012.
53. 53. Turkish Food Codex. (2019). *Meat, prepared meat mixtures and meat products communiqué* (No. 2018/52). Official Gazette, 30670, 29 January 2019.
54. 54. Uzunlu, S. (2019). Assessment of some physicochemical and microbiological quality parameters of raw meatballs prepared with high pressurized meat. *Gıda (Food)*, *44*(2), 340–347.
55. 55. Valero, A., Pérez-Rodríguez, F., Carrasco, E., Fuentes-Alventosa, J. M., García-Gimeno, R. M., & Zurera, G. (2009). Modelling the growth boundaries of *S. aureus*: Effect of temperature, pH and water activity. *International Journal of Food Microbiology*, 133(1–2), 186–194.
56. 56. Valík, Ľ., Medveďová, A., Bajúsová, B., & Liptáková, D. (2008). Variability of growth parameters of *S. aureus* in milk. *Journal of Food & Nutrition Research*, *47*(1).
57. 57. Wang, J., Koseki, S., Chung, M. J., & Oh., D. H. (2017). A novel approach to predict the growth of *Staphylococcus aureus* on rice cake. *Frontiers in Microbiology, 8*, 1140. https://doi.org/10.3389/fmicb.2017.01140.
58. 58. Xie, Z., Peng, Y., Li, C., Luo, X., Wei, Z., Li, X., Yao, Y., Fang, T. & Huang, L. (2020). Growth kinetics of *S. aureus* and background microorganisms in camel milk. *Journal of dairy science*, 103(11), 9958–9968.
59. 59. Zhou, C., & Fey, P. D. (2020). The acid response network of *S. aureus*. *Current opinion in microbiology*, 55, 67–73.
60. 60. Ziane, M., & Membré, J. M. (2022). A second-order Monte Carlo simulation model to describe coagulase-positive Staphylococci growth in mayonnaise served in Algerian pizzerias. *Microbial Risk Analysis*, 20, 100187.
61. 61. Zor, M., Erdemir, E., Fettahoğlu, K., Topdaş, E. F., & Şengül, M. (2025). Physicochemical properties, volatile compound profile changes, and sensory evaluation of meatballs with the addition of different vegetable peels. *Italian Journal of Food Science/Rivista Italiana di Scienza degli Alimenti*, *37*(3).

Figures

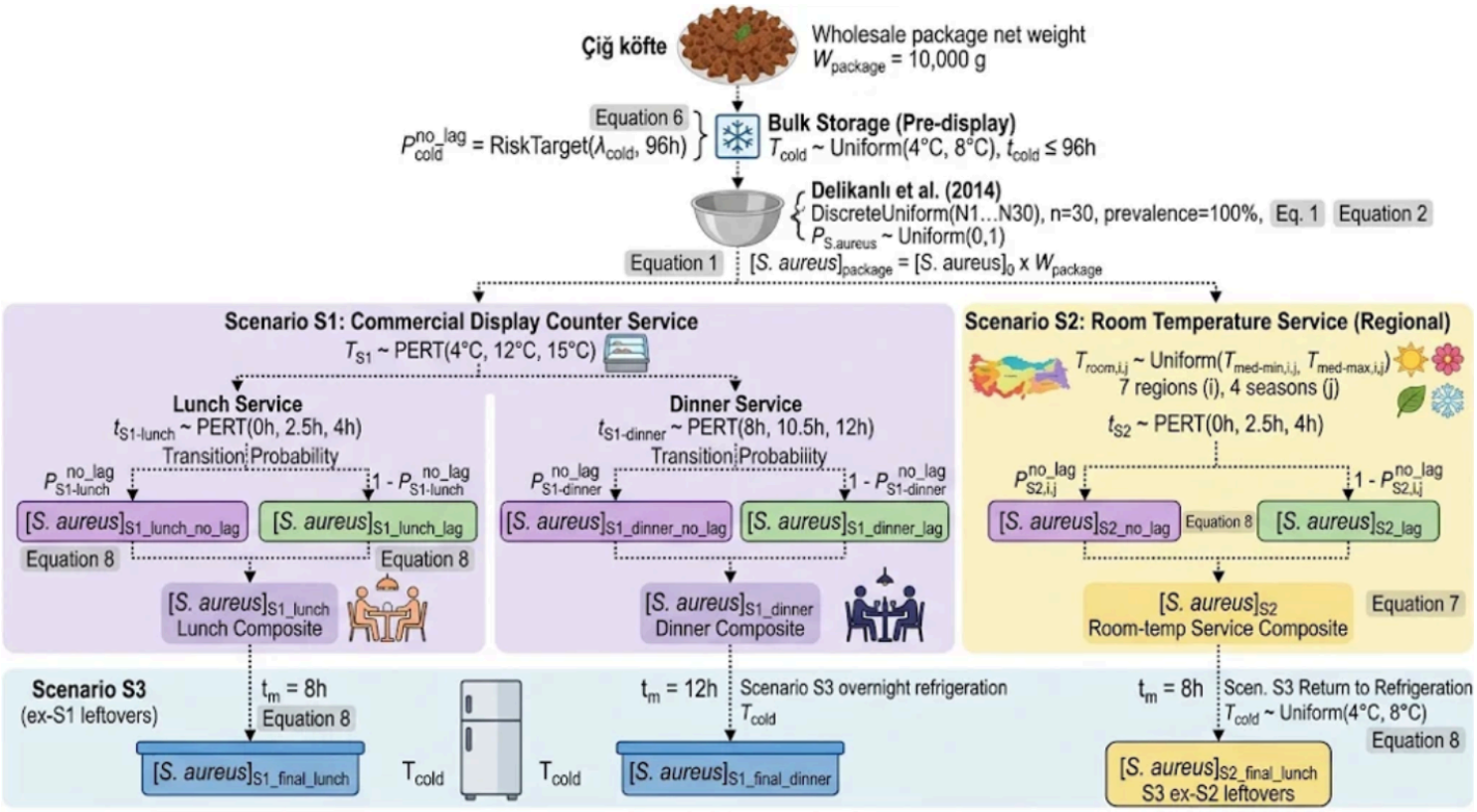

Figure 1

Overview of the *çiğ köfte* retail and consumption scenarios with corresponding time and temperature conditions.

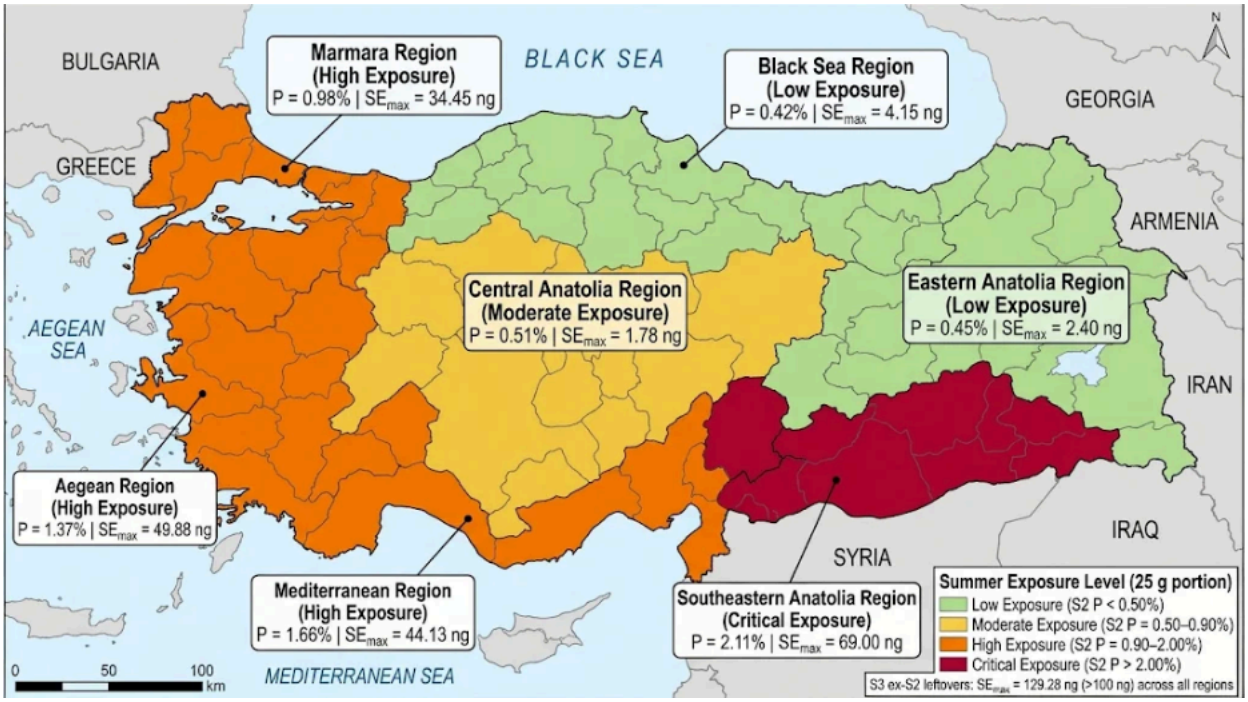

Figure 2

Spatiotemporal exposure map of S. aureus critical threshold exceedance [P(C≥5.0 〖log_10"CFU g" 〗^(-1))] and maximum staphylococcal enterotoxin yield (〖"SE" 〗_max, ng per 25 g meatball) in plant-based çiğ köfte across the seven geographical regions of Türkiye during summer under direct ambient service (Scenario S2) and subsequent refrigerated leftover storage (Scenario S3 ex-S2, where 〖"SE" 〗_max=129.28 "ng/meatball">100 "ng " across all regions).